



Dynamic analysis of a spherical sandwich sector with piezoelectric face sheets and FG-CNT core subjected to low-velocity impact

Hamed Raissi¹

Received: 10 December 2020 / Accepted: 9 June 2021 / Published online: 24 June 2021
© The Brazilian Society of Mechanical Sciences and Engineering 2021

Abstract

Time-dependent analysis based on layerwise theory (LT) along with higher-order shear deformation theory (HSDT) is studied to determine the stress distribution in a simply supported sector of spherical sandwich shell with piezoelectric face sheets and functionally graded carbon nanotube (FG-CNT) core subjected to the low-velocity impact. The aim of the current study is the investigation of the dynamic analysis of the sandwich sector when the spherical elastic ball hits the top face sheet of sector with an initial velocity of 50 m/s. The classical non-adhesive elastic contact theory and Hunter's relationship are used to calculate the normal contact pressure distribution in terms of time, as well as a function of distance from the center of contact location. The out-of-shell displacement of the sandwich shell at each layer is assumed to be a quadratic polynomial function of the radial component in addition to a function of the coordinate components within the shell. This means that the normal out-of-shell strain changes in the form of a linear function along with the thickness of each layer. The nineteen equations of motion are obtained by using Hamilton's principle, Maxwell's static equation. The numerical method was used to solve the nineteen equations of motion based on the finite difference method. The results show that the mechanical properties of FG-CNT have more effect on the stress distribution in the sandwich sector. Moreover, the variation of the voltage in terms of time caused by the impact of the spherical elastic ball was calculated.

Keywords Low-velocity impact · Layerwise theory · Classical non-adhesive elastic contact theory · Spherical sandwich shell · Maxwell's static equation

List of symbols

a	The radius of the contact area	F	The applied force
a_{\max}	The maximum radius of the contact area	F_{\max}	The maximum contact force
C_{ij}	The elastic constant of the piezoelectric layer ($i, j = 1, 2, 3$)	G_{ij}^{CNT}	The shear modulus of the FG-CNT ($i, j = 1, 2, 3$)
d	The contact depth	G^m	The shear modulus of the matrix
D_i	The electric displacement components ($i = 1, 2, 3$)	M_0	The mass of the spherical ball
d_{\max}	The maximum contact depth	P_0	The maximum contact pressure
E_0	The elastic moduli of the spherical ball	$Q_{ij}^{(2)}$	The core stiffness tensor ($i, j = 1, 2, 3$)
E_{eff}	The effective elastic modulus	$r^{(1)}$	The radius of the middle layer of the bottom face sheet
E_i	The electric field density ($i = 1, 2, 3$)	$r^{(2)}$	The radius of the middle layer of the core
e_{ij}	The piezoelectric constant ($i, j = 1, 2, 3$)	$r^{(3)}$	The radius of the middle layer of the top face sheet
E_{ii}^{CNT}	The elastic modulus of the FG-CNT ($i, j = 1, 2, 3$)	R_{eff}	The effective radius.
E^m	The elastic modulus of the matrix	t_{\max}	The impact time duration
		u_0	The displacement of the core's mid-surface along ξ_1
		$u_1^{(k)}$	The displacement components along ξ_1
		$u_2^{(k)}$	The displacement components along ξ_2
		$u_3^{(k)}$	The displacement components along ξ
		v_0	The displacement of the core's mid-surface along ξ_2

Technical Editor: Marcelo Areias Trindade.

✉ Hamed Raissi
hamedraissi@yahoo.com

¹ Department of Mechanical Engineering, Shahid Chamran University of Ahvaz, P.O. Box 6135783151, Ahvaz, Iran

V_0	The initial velocity of the spherical ball
V^m	The volume fraction of the matrix
V_{CNT}	The volume fraction of the FG-CNT
w_0	The displacement of the core's mid-surface along ξ
W^{CNT}	The mass fraction of the FG-CNT
Γ	The Gamma function
δK	The virtual kinetic energy
δU	The virtual strain energy
δW	The virtual work
η_1	The efficiency CNT/matrix parameter number 1
η_2	The efficiency CNT/matrix parameter number 2
η_3	The efficiency CNT/matrix parameter number 3
μ_i	The dielectric constant ($i = 1, 2, 3$)
ν_0	The Poisson's ratio of the spherical ball
ν^m	The Poisson's ratio of the matrix
ν_{ij}^{CNT}	The Poisson's ratio of the FG-CNT ($i, j = 1, 2, 3$)
ρ^{CNT}	The density of the FG-CNT
$\Phi^{(k)}$	The electric potential ($k = 1, 3$)

1 Introduction

The use of the piezoelectric materials, as well as FG-CNT structures in various fields in energy storage, molecular electronics, thermal materials, electrical conductivity, air and water filtration, conductive adhesive, and biomedical, is expanding. The piezoelectric material is a special type of dielectric material which simultaneously comprises two branches of elasticity and electricity.

Due to the complexity of the dynamic behavior of the piezoelectric materials as well as FG-CNT when the structures are subjected to low-velocity impact, there is an interest to study these materials. Various scientific articles have been investigated in the field of low-velocity impact. Cestino et al. [1] studied buckling behavior and stress analysis of a circular plate after low-velocity impact, experimentally, and numerically. In this investigation, the tensile load, impact energy, and residual stress were calculated. There was a good agreement between the results. Bikakis [2] studied dynamic response analysis of Glare plates subjected to low-velocity impact, theoretically. In this research, the results to determine the contact force were compared to those obtained by experimental tests. Yellur et al. [3] studied the thermo-plastic analysis of a rectangular sandwich plate with honeycomb core subjected to low-velocity impact, experimentally. In this study, the contact force, energy observation, and stress distribution were calculated in terms of time. Saleh et al. [4] studied a three-dimensional study of the low-velocity impact on a rectangular plate. In this study, the contact force was calculated as a function of the plate's deformation. Kareem and Majeed [5] studied the transient dynamic analysis of a

spherical shell subjected to the low-velocity impact, experimentally, and numerically. The equations of motion were obtained by using HSDT and Hamilton's principle. The results of the numerical solution to calculate the contact force and deflection were compared to those obtained by experimental tests. Gao et al. [6] studied the low-velocity impact on a sandwich plate with a honeycomb core. In this paper, the effect of honeycomb shape on energy observation was calculated, theoretically. Mohammed et al. [7] studied the stress analysis of a rectangular sandwich plate with a foam core subjected to the low-velocity impact, experimentally, and numerically. In this investigation, the maximum contact force and stress distribution of the plate were calculated. Mao et al. [8] studied the nonlinear dynamic response of the FG spherical shell subjected to low-velocity impact. In this research, the equations of motion were derived by using Giannakopoulos's 2D contact model, first-order shear deformation theory (FSDT), and Hamilton's principle. Lei and Tong [9] studied stress analysis of a simply supported FG-CNT cylindrical shell subjected to the low-velocity impact, theoretically. In this research, the classic shell theory was used and the impact load was considered as the Fourier series. In addition, the effects of temperature, length, and thickness of the shell on the impact force and deflection of the shell were calculated.

Khodadadi et al. [10] studied the failure analysis of an aluminum-rubber sandwich plate subjected to the impact of a hemispherical impactor. In this paper, the numerical results obtained by LS-DYNA were compared to those obtained by experimental tests. Sy et al. [11] studied the low-velocity impact behavior of a flax-epoxy laminate plate, experimentally. The results of experimental tests to determine contact forces were compared with those obtained by LS-DYNA. Erklig and Dogan [12] studied stress analysis of a rectangular hybrid nano-composite plate subjected to the low-velocity impact, experimentally. In this investigation, the effects of the ply-angle orientation, and thickness of the plate as well as the energy of the impact on the stress components, impact force, and deflection of the plate were calculated. Yao et al. [13] studied the failure analysis of a circular composite plate subjected to low-velocity impact. In this study, by using Abaqus software and experimental tests, the impact force and energy observation were calculated. Guo et al. [14] studied dynamic analysis of a bolted joint in a rectangular composite plate subjected to low-velocity impact. In this investigation, Abaqus software was used and the effect of impact location on the stress distribution was calculated. Meo et al. [15] studied the dynamic response of the rectangular sandwich plate with honeycomb core subjected to the low-velocity impact experimentally. In this investigation, the contact force was calculated in terms of the energy observation. Sun et al. [16] studied the dynamic response of a circular sandwich plate subjected to low-velocity impact,

experimentally. In this paper, the contact force and energy observation were calculated in terms of the plate's displacement. Gunes and Sahin [17] studied the effect of surface crack on the dynamic response of a rectangular hybrid laminated composite plate subjected to the low-velocity impact, experimentally. In this study, the effects of the geometry of the plate and the energy of the impact on the impact force and deflection of the plate were studied.

He et al. [18] studied failure analysis of a clamped circular sandwich plate with X-frame core subjected to low-velocity impact. In this research, by using Abaqus software as well as experimental tests, the contact force, and energy observation in terms of time were calculated. Dai et al. [19] studied dynamic analysis of a rectangular sandwich plate with honeycomb core subjected to low-velocity impact, experimentally. In this research, the effect of impact energy on the contact force, impact duration, and deformation of the plate was investigated. Yuan et al. [20] studied dynamic analysis of a carbon fiber composite plate subjected to low-velocity impact, experimentally. In this research, the effect of the ply-angle laminate on the contact force was calculated. He et al. [21] studied the low-velocity impact of a rectangular sandwich plate with a honeycomb core, numerically, and experimentally. In this investigation, the effects of the thickness of honeycomb as well as the impact velocity were studied to determine the contact force and the energy observation in terms of time. Sohel et al. [22] studied dynamic analysis of a column subjected to impact loads. In this investigation, the numerical solution based on a finite element analysis was done and the results were compared to those obtained by experimental tests. Moreover, deflection of the column was calculated in terms of time and initial velocity. Sadeghpour et al. [23] studied the stress analysis of a curved sandwich beam with a foam core subjected to the low-velocity impact, theoretically. In this study, the maximum deflection of the beam, the variation of projective velocity, and the contact force were calculated in terms of time. Fan et al. [24] studied the dynamic analysis of a laminated beam with FG-CNT layers rested on the viscoelastic foundation subjected to low-velocity impact. In this investigation, the maximum contact force as well as the maximum deflection of beam were compared to those obtained by the previous study. Xu et al. [25] studied experimental and numerical investigations on a rectangular composite plate with shape memory alloy layers subjected to low-velocity impact. In this research, experimental tests and finite element method were used to determine the contact force. Nasrin and Ibrahim [26] studied the dynamic analysis of a beam with an initial crack subjected to low-velocity impact, numerically, and experimentally. In this investigation, the beam deflection as well as the failure analysis of the beam were calculated. Manohar et al. [27] carried out some experimental tests to study the dynamic analysis of a composite plate. In this study, the drop test

was carried out and the collision energy and deflection of the plate were calculated.

Various studies have been carried out in the field of LT. In most studies, it has been assumed that the out-of-plate or out-of-shell displacement is an independent function of the vertical component of the coordinate system defined along with thickness of the plate or shell. Hosseini and Kolahchi [28] used LT along with third-order shear deformation theory (TSDT) to study the dynamic analysis of a cylindrical FG-CNT shell subjected to the earthquake load. Cong et al. [29] studied LT along with TSDT to determine the nonlinear dynamic response of a curved sandwich shell subjected to blast pressure. Raissi [30, 31] studied LT along with HSDT to determine the stress distribution in the cylindrical and spherical sandwich shells with piezoelectric face sheets and FG-CNT core subjected to blast pressure. Romera et al. [32] studied LT along with FSDT to determine the stress distribution in a rectangular composite plate subjected to a tensile load. Malikan and Nguyen [33] studied buckling analysis of a rectangular piezo-magneto-electric nano-plate subjected to a hygro-thermal environment and external voltage. In this investigation, LT along with FSDT was used. Van et al. [34] studied LT along with FSDT to determine the stress distribution in a three-layer sandwich plate rested on the viscoelastic foundation subjected to a moving mass.

The main topic that will be examined in the present study is the effect of the low-velocity impact on the stress components in a sector of the spherical sandwich shell. The spherical sandwich shell is made in such a way that there are two piezoelectric layers in the face sheets, and it also has an FG-CNT core. Layerwise theory, Hamilton's principle, the classical non-adhesive elastic contact theory, and Hunter's relationship are used to determine the equations of motion. Raissi [30, 31] studied the stress distribution in a sector of the spherical and cylindrical sandwich shells with piezoelectric face sheets and FG-CNT core subjected to blast pressure. The difference between the current paper with those carried out in Refs. [30, 31] is that in the current investigation, the issue of the low-velocity impact will be studied but in Refs. [30, 31], the blast phenomena in the sector of the spherical and cylindrical sandwich shells with piezoelectric face sheets and FG-CNT core had been investigated. In addition, Raissi et al. [35] studied LT along with FSDT to study the stress distribution in a five-layer sandwich plate subjected to static pressure. It can be seen that the present study is completely different from the paper mentioned in Ref. [35]. Neves et al. [36, 37] used LT along with sinusoidal and hyperbolic sinusoidal shear deformation theories to calculate the free vibration analysis of the FG plate. In these investigations, the transverse displacement was considered as a quadratic in the thickness direction.

It is noteworthy that the innovation of the present study is in three issues. Definition of the problem of the effect of the

low-velocity impact on a sector of the sandwich spherical shell with two piezoelectric face sheets and one FG-CNT core is the first innovation. In addition, the physical model of the impact of the spherical ball with the spherical sandwich shell is approximated as a mathematical model based on the classical non-adhesive elastic contact theory and Hunter’s relationship. So far, there has been no research in this regard.

According to the mention references, there is a variety of LT along with higher-order shear deformation theory on the subject of impact, but few papers [36, 37] have examined the vertical displacement of the shell as a quadratic function along the thickness direction. The reason for this is the enormous intensity of the volume of the equations and how to solve them. In addition, the complex behavior of FG-CNT as well as the extraordinary piezoelectric behavior will further complicate the problem. The use of layerwise theory along with higher-order shear deformation theory in the problem of low-velocity impact is the second innovation. Furthermore, it is assumed that the out-of-shell displacement in the face sheets and core of the sandwich shell is assumed to be a second-order polynomial function of the thickness of the layers. This means that the normal strain changes in the form of a linear function along with the thickness of the layer.

Finally, the third innovation that consists of two prior innovations, the simultaneous solving of the dynamic

equations will be defined as a function in terms of time. It is noteworthy that according to the classical non-adhesive elastic contact theory, the normal contact pressure distribution is defined as a relationship in terms of time, as well as a function of distance from the center of the contact location. Therefore, the normal contact pressure is defined as the combination of a sinusoidal function in terms of time as well as a radical function in terms of distance from the center of the contact location. Hamilton’s principle and Maxwell’s static equation are used to obtain the equations of motion.

Therefore, the present investigation tries to present a new theoretical solution based on layerwise theory along with higher-order shear deformation theory and Hamilton’s principle to study the dynamic behavior of the three-layer spherical sandwich sector with piezoelectric face sheets and FG-CNT core subjected to the low-velocity impact.

2 The geometry and material properties of the sandwich shell

Figure 1 shows a simply supported spherical sandwich shell with two piezoelectric face sheets and one FG-CNT core. The sandwich shell is subjected to the low-velocity impact of

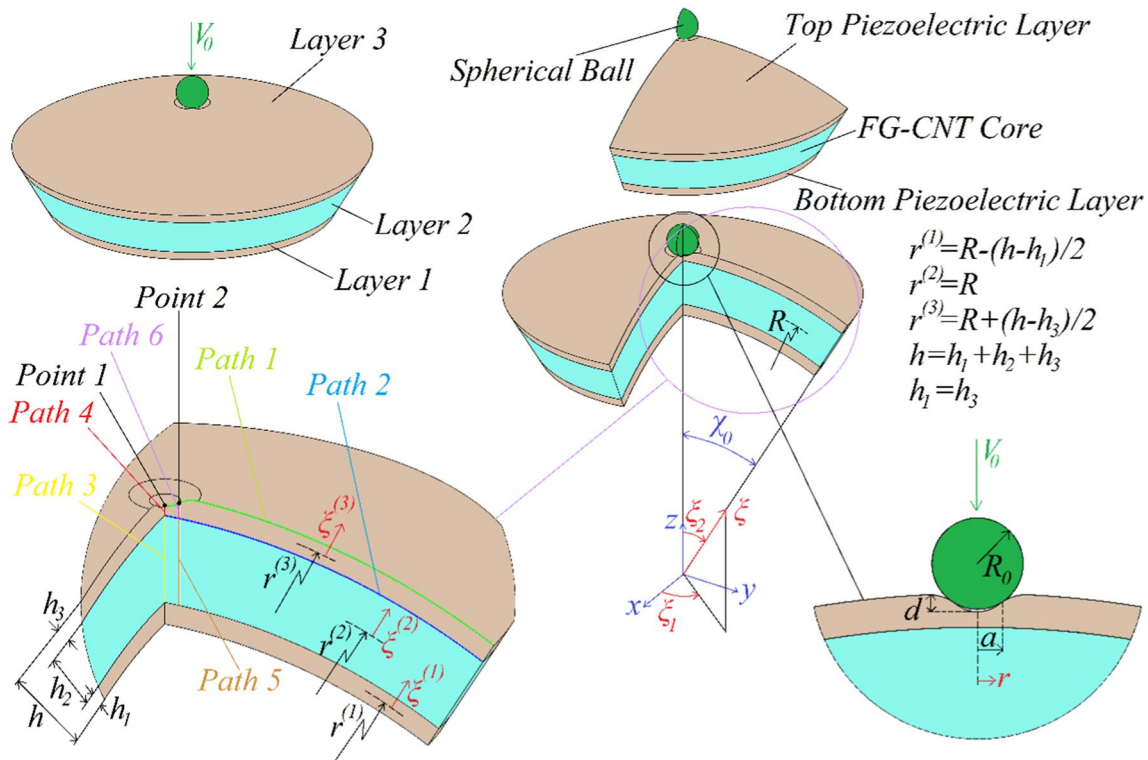
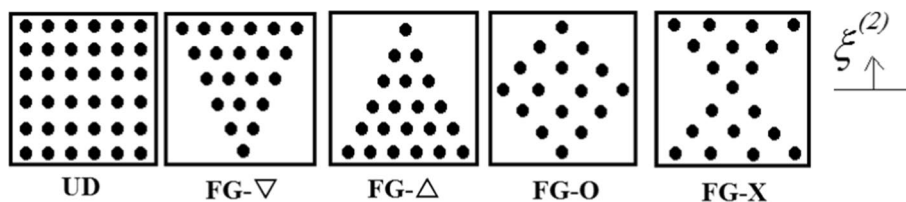


Fig. 1 The simply supported sector of the spherical sandwich shell with FG-CNT core and piezoelectric face sheets subjected to low-velocity impact

Fig. 2 The shape of the FG-CNT samples in the matrix



the spherical ball that hits on its top face sheet. It is assumed that no separation will have occurred between the layers.

The variation in modulus of elasticity, Poisson’s ratio, and density of the FG-CNT core along its thickness are defined by Eqs. (A1)–(A11) presented in “Appendix A”. The stress analysis is performed for the five FG-CNT samples as FG-UV, FG-∇, FG-Δ, FG-O, and FG-X. Moreover, Fig. 2 shows the shape of the five samples of FG-CNT defined in the current study for the core of the sandwich sector. As mentioned in Eqs. (A1)–(A11), the direction of the functionally graded nano-carbon layers is defined so that they are located in the circular direction of the spherical shell (ξ_1 direction).

3 Derivation of governing equations

Based on HSDT, the displacement components in the thickness direction for each layer change according to the higher-order shear deformation theory. The displacement components in the sandwich plate are given in Eqs. (B1)–(B9) presented in “Appendix B”.

For a simply supported spherical sandwich shell, the displacement components and curvatures ($u_0, v_0, w_0, \psi_i^{(k)}, \alpha_i^{(k)}, \beta_j^{(k)}$ and $\lambda_j^{(k)}$ ($i = 1, 2, 3; j = 1, 2$ and $k = 1, 2, 3$)) can be introduced by Eqs. (C1)–(C13) presented in “Appendix C.”

Based on linear elasticity, the strain components in the k th layer can be written in terms of displacements, as shown in Eq. (1). According to Fig. 1, $r^{(k)}$ defined in Eq. (1) represents the radius of the middle layer of the bottom face sheet, the core, and the top face sheet for values of k from one to three, respectively. Substituting for displacement components from Eqs. (B1)–(B9) presented in “Appendix B,” the strain vector in each layer can be written in terms of $u_0, v_0, w_0, \psi_i^{(k)}, \alpha_i^{(k)}, \beta_j^{(k)}$, and $\lambda_j^{(k)}$ ($i = 1, 2, 3; j = 1, 2$ and $k = 1, 2, 3$).

$$\left\{ \begin{aligned} \varepsilon_1^{(k)} &= \frac{1}{r^{(k)} \sin \xi_2^{(k)}} \frac{\partial u_1^{(k)}}{\partial \xi_1^{(k)}} + \frac{1}{r^{(k)}} u_3^{(k)} + \frac{1}{r^{(k)}} u_2^{(k)} \cot \xi_2^{(k)}; \\ \varepsilon_2^{(k)} &= \frac{1}{r^{(k)}} \frac{\partial u_2^{(k)}}{\partial \xi_2^{(k)}} + \frac{1}{r^{(k)}} u_3^{(k)}; \\ \varepsilon_3^{(k)} &= \frac{\partial u_3^{(k)}}{\partial \xi_3^{(k)}}; \\ \gamma_{23}^{(k)} &= \frac{\partial u_2^{(k)}}{\partial \xi_3^{(k)}} + \frac{1}{r^{(k)}} \frac{\partial u_3^{(k)}}{\partial \xi_2^{(k)}} - \frac{1}{r^{(k)}} u_2^{(k)}; \\ \gamma_{13}^{(k)} &= \frac{1}{r^{(k)} \sin \xi_2^{(k)}} \frac{\partial u_3^{(k)}}{\partial \xi_1^{(k)}} + \frac{\partial u_1^{(k)}}{\partial \xi_3^{(k)}} - \frac{1}{r^{(k)}} u_1^{(k)}; \\ \gamma_{12}^{(k)} &= \frac{1}{r^{(k)} \sin \xi_2^{(k)}} \frac{\partial u_1^{(k)}}{\partial \xi_1^{(k)}} + \frac{1}{r^{(k)}} \frac{\partial u_1^{(k)}}{\partial \xi_2^{(k)}} - \frac{1}{r^{(k)}} u_1^{(k)} \cot \xi_2^{(k)}; \end{aligned} \right. \quad (1)$$

Based on Hooke’s principle, the stress–strain relation in FG-CNT core and piezoelectric face sheets can be written as Eqs. (D1) and (D2) ($k = 1$ and 3) presented in “Appendix D,” respectively. Moreover, the electric displacement relations for piezoelectric face sheets can be written as Eq. (D3). In this study, the electric potential ($\Phi^{(k)}$) for the first and third layers of the sandwich shell is assumed as Eq. (2). The reason for choosing this value of the electric potential is that the voltage in the middle layer of the piezoelectric face sheets ($\xi^{(1)} = 0$ or $\xi^{(3)} = 0$) is not considered zero and at the same time it is considered zero in the innermost and outermost layers ($\xi^{(i)} = -h_i/2$ or $\xi^{(i)} = h_i/2, i = 1$ or 3). In addition, it is essential to choose the electrical potential that satisfied the Maxwell equation. Moreover, this value of the electric potential distribution was used for the electrical potential in Refs. [30, 31]. Furthermore, a similar distribution of the electric potential was presented in Refs. [38, 39].

$$\Phi^{(k)}(\xi_1, \xi_2, \xi^{(k)}, t) = \begin{cases} \varphi^{(3)}(\xi_1, \xi_2, t) \cos\left(\frac{\pi \xi^{(3)}}{h_3}\right) & \text{Top piezoelectric layer} \\ \varphi^{(1)}(\xi_1, \xi_2, t) \cos\left(\frac{\pi \xi^{(1)}}{h_1}\right) & \text{Bottom piezoelectric layer} \end{cases} \quad ; \text{ where : } k = 1 \text{ or } 3. \quad (2)$$

It is noteworthy that the electrical fields of the piezoelectric layers affect the resin of the core [40–43]. According to Refs. [40–43], it can be observed that by applying a certain value of the electrical voltage to the resin, there is a possibility of mechanical failure in the resin. In the current study, the effect of the electrical fields on the mechanical behavior of the resin used in the core has been neglected.

In order to generate the equations of motion, Hamilton’s principle is used as Eq. (3). In this equation, δK , δU , and δW are virtual kinetic energy, virtual strain energy, and virtual work due to the external forces, respectively.

$$\int_0^T \delta L dt = \int_0^T [\delta K - (\delta U - \delta W)] dt = 0 \tag{3}$$

Equation (4) shows how to calculate the virtual kinetic energy. Equation (E1) presented in “Appendix E” can be derived for the virtual kinetic energy by simplifying Eq. (4) and classifying component by component,

$$\delta K = \int_V \sum_{k=1}^3 \rho^{(k)} \left(\dot{u}_1^{(k)} \delta \dot{u}_1^{(k)} + \dot{u}_2^{(k)} \delta \dot{u}_2^{(k)} + \dot{u}_3^{(k)} \delta \dot{u}_3^{(k)} \right) dV \tag{4}$$

Equation (5) shows how to calculate the virtual strain energy. By simplifying Eq. (5) and classifying component by component, Eq. (E2) presented in “Appendix E” can be calculated for the virtual strain energy.

$$\delta U = \int_V \sigma_{ij} \varepsilon_{ij} dV \tag{5}$$

In order to calculate the virtual work, it is necessary to determine the normal contact pressure distribution resulting from the collision of the spherical ball when it hits the top face sheet in terms of time. According to Fig. 1, the spherical ball hits the top face sheets of the sector with initial velocity V_0 . According to the classical non-adhesive elastic contact theory, the radius of the contact area and the applied force can be defined as Eqs. (6a) and (6b), respectively.

$$a = \sqrt{R_{\text{eff}} d} \tag{6a}$$

$$F = K d^{\frac{3}{2}} \quad \text{where } K = \frac{4}{3} E_{\text{eff}} R_{\text{eff}}^{\frac{1}{2}} \tag{6b}$$

In addition, the effective radius and the effective elastic modulus can be defined as Eqs. (6c) and (6d), respectively.

$$R_{\text{eff}} = \frac{\left(R + \frac{h}{2} \right) R_0}{R + R_0 + \frac{h}{2}} \tag{6c}$$

$$E_{\text{eff}} = \left(\frac{1 - \nu_{12}^{(3)^2}}{E_{11}^{(3)}} + \frac{1 - \nu_0^2}{E_0} \right)^{-1} \tag{6d}$$

Due to the initial velocity of the spherical ball (V_0), the maximum contact depth, the maximum radius of the contact area, the maximum contact force, the maximum normal contact pressure, and the impact time duration are calculated as Eqs. (7a)–(7e), respectively.

$$d_{\text{max}} = \left(\frac{5}{4} \frac{V_0^2}{K' K} \right)^{\frac{2}{5}} \quad \text{where } K' = \frac{1}{M_0} \tag{7a}$$

$$a_{\text{max}} = \sqrt{R_{\text{eff}} d_{\text{max}}} \tag{7b}$$

$$F_{\text{max}} = K d_{\text{max}}^{\frac{3}{2}} \tag{7c}$$

$$P_0 = \frac{3F_{\text{max}}}{2\pi a_{\text{max}}^2} \tag{7d}$$

$$t_{\text{max}} = \frac{4}{5} \sqrt{\pi} \frac{\Gamma\left(\frac{2}{5}\right)}{\Gamma\left(\frac{9}{10}\right)} \frac{d_{\text{max}}}{V_0} \tag{7e}$$

According to Hunter’s relationship, the maximum force can be approximated in terms of time as Eq. (8a). The maximum normal contact pressure distribution in terms of time and distance of the center of impact line (see Fig. 1) due to Hunter’s relationship can be defined as Eq. (8b).

$$F = F_{\text{max}} \sin\left(\frac{\pi t}{t_{\text{max}}}\right) \tag{8a}$$

$$P = P_0 \sin\left(\frac{\pi t}{t_{\text{max}}}\right) \sqrt{1 - \frac{r^2}{a_{\text{max}}^2}} \tag{8b}$$

Based on the contact pressure presented in Eq. (8b), the virtual work can be derived by Eq. (9). By inserting Eqs. (E1), (E3) and (9) into Eq. (3) and classifying relations, the seventeen equations can be obtained from (10a)–(10q).

$$\delta W = \int_0^{2\pi} \int_0^{a_{\text{max}}} P(t) \delta u_3^{(3)} r dr d\xi_1 \Rightarrow \tag{9}$$

$$\delta W = \frac{2\pi}{3} P_0 a_{\text{max}}^2 \sin\left(\frac{\pi t}{t_{\text{max}}}\right) \delta u_3^{(3)}$$

$$\delta u_0 : \sum_{k=1}^3 \left(\frac{1}{r^{(k)}} \left[\frac{1}{\sin \xi_2} \frac{\partial N_{11}^{(k)}}{\partial \xi_1} - N_{13}^{(k)} + \frac{\partial N_{12}^{(k)}}{\partial \xi_2} - N_{12}^{(k)} \cot \xi_2 \right] \right)$$

$$= \left\{ \begin{aligned} & \left(I_0^{(1)} + I_0^{(2)} + I_0^{(3)} \right) \ddot{u}_0 + \left(-\frac{h_1}{3} I_0^{(1)} + I_1^{(1)} - \frac{4}{3h_2^2} I_3^{(1)} \right) \ddot{\psi}_1^{(1)} + \left(-\frac{h_2}{3} I_0^{(1)} + I_1^{(2)} - \frac{4}{3h_2^2} I_3^{(2)} + \frac{h_2}{3} I_0^{(3)} \right) \ddot{\psi}_1^{(2)} + \left(\frac{h_3}{3} I_0^{(3)} + I_1^{(3)} - \frac{4}{3h_2^2} I_3^{(3)} \right) \ddot{\psi}_1^{(3)} \\ & - \left(\frac{h_1^2}{8} I_0^{(1)} + \frac{1}{2} I_2^{(1)} \right) \ddot{\alpha}_1^{(1)} - \left(\frac{h_2^2}{8} I_0^{(1)} + \frac{1}{2} I_2^{(2)} + \frac{h_2^2}{8} I_0^{(3)} \right) \ddot{\alpha}_1^{(2)} - \left(\frac{h_3^2}{8} I_0^{(3)} + \frac{1}{2} I_2^{(3)} \right) \ddot{\alpha}_1^{(3)} + \left(\frac{h_1^3}{24} I_0^{(1)} - \frac{1}{3} I_3^{(1)} \right) \ddot{\lambda}_1^{(1)} \\ & + \left(\frac{h_2^3}{24} I_0^{(1)} - \frac{1}{3} I_3^{(2)} - \frac{h_2^3}{24} I_0^{(3)} \right) \ddot{\lambda}_1^{(2)} - \left(\frac{h_3^3}{24} I_0^{(3)} + \frac{1}{3} I_3^{(3)} \right) \ddot{\lambda}_1^{(3)} - \frac{8}{3h_1^2} I_0^{(1)} \ddot{\beta}_1^{(1)} - \frac{4}{3h_2^2} \left(I_0^{(1)} + I_0^{(2)} + I_0^{(3)} \right) \ddot{\beta}_1^{(2)} - \frac{8}{3h_2^2} I_0^{(3)} \ddot{\beta}_1^{(3)} \end{aligned} \right\} \quad (10a)$$

$$\delta \psi_1^{(1)} : \left(\begin{aligned} & -\frac{h_1}{3r^{(1)}} \left[\frac{1}{\sin \xi_2} \frac{\partial M_{11}^{(1)}}{\partial \xi_1} + \frac{\partial M_{12}^{(1)}}{\partial \xi_2} \right] - \frac{1}{r^{(1)}} \left[\frac{1}{\sin \xi_2} \frac{\partial M_{11}^{(1)}}{\partial \xi_1} + \frac{\partial M_{12}^{(1)}}{\partial \xi_2} - \frac{4}{3h_1^2} \left(\frac{1}{\sin \xi_2} \frac{\partial q_{11}^{(1)}}{\partial \xi_1} + \frac{\partial q_{12}^{(1)}}{\partial \xi_2} \right) \right] \\ & + \left[\left(1 + \frac{h_1}{3r^{(1)}} \right) N_{13}^{(1)} + \frac{h_1}{3r^{(1)}} N_{12}^{(1)} \cot \xi_2 - \frac{4}{h_1^2} P_{13}^{(1)} \right] + \frac{1}{r^{(1)}} \left[M_{13}^{(1)} + M_{12}^{(1)} \cot \xi_2 - \frac{4}{3h_1^2} \left(q_{13}^{(1)} + q_{12}^{(1)} \cot \xi_2 \right) \right] \end{aligned} \right)$$

$$= \left\{ \begin{aligned} & \left(-\frac{h_1}{3} I_0^{(1)} + I_1^{(1)} - \frac{4}{3h_2^2} I_3^{(1)} \right) \ddot{u}_0 + \left(\frac{h_1^2}{9} I_0^{(1)} - \frac{2h_1}{3} I_1^{(1)} + I_2^{(1)} + \frac{8}{9h_1^3} I_3^{(1)} - \frac{8}{3h_2^2} I_4^{(1)} + \frac{16}{9h_1^4} I_6^{(1)} \right) \ddot{\psi}_1^{(1)} - \frac{h_2}{3} \left(-\frac{h_1}{3} I_0^{(1)} + I_1^{(1)} - \frac{4}{3h_2^2} I_3^{(1)} \right) \ddot{\psi}_1^{(2)} \\ & + \left(\frac{h_1^3}{24} I_0^{(1)} - \frac{h_1^2}{8} I_1^{(1)} + \frac{h_1}{6} I_2^{(1)} - \frac{1}{3} I_3^{(1)} + \frac{2}{3h_1^2} I_5^{(1)} \right) \ddot{\alpha}_1^{(1)} - \frac{h_2^2}{8} \left(-\frac{h_1}{3} I_0^{(1)} + I_1^{(1)} - \frac{4}{3h_2^2} I_3^{(1)} \right) \ddot{\alpha}_1^{(2)} - \frac{1}{3} \left(\frac{h_1^4}{24} I_0^{(1)} - \frac{h_1^3}{8} I_1^{(1)} - \frac{h_1}{6} I_2^{(1)} + I_3^{(1)} - \frac{4}{3h_1^2} I_5^{(1)} \right) \ddot{\lambda}_1^{(1)} \\ & + \frac{h_2^3}{24} \left(-\frac{h_1}{3} I_0^{(1)} + I_1^{(1)} - \frac{4}{3h_2^2} I_3^{(1)} \right) \ddot{\lambda}_1^{(2)} - \frac{8}{3h_1^2} \left(-\frac{h_1}{3} I_0^{(1)} + I_1^{(1)} - \frac{4}{3h_2^2} I_3^{(1)} \right) \ddot{\beta}_1^{(1)} - \frac{4}{3h_2^2} \left(-\frac{h_1}{3} I_0^{(1)} + I_1^{(1)} - \frac{4}{3h_2^2} I_3^{(1)} \right) \ddot{\beta}_1^{(2)} \end{aligned} \right\} \quad (10b)$$

$$\delta \psi_1^{(2)} : \left(\begin{aligned} & \frac{h_2}{3 \sin \xi_2} \left[\frac{1}{r^{(1)}} \frac{\partial N_{11}^{(1)}}{\partial \xi_1} - \frac{1}{r^{(3)}} \frac{\partial N_{11}^{(3)}}{\partial \xi_1} \right] + \frac{h_2}{3} \left[\frac{1}{r^{(1)}} \frac{\partial N_{12}^{(1)}}{\partial \xi_2} - \frac{1}{r^{(3)}} \frac{\partial N_{12}^{(3)}}{\partial \xi_2} \right] - \frac{1}{r^{(2)}} \left[\frac{1}{\sin \xi_2} \frac{\partial M_{11}^{(2)}}{\partial \xi_1} + \frac{\partial M_{12}^{(2)}}{\partial \xi_2} - \frac{4}{3h_2^2} \left(\frac{1}{\sin \xi_2} \frac{\partial q_{11}^{(2)}}{\partial \xi_1} + \frac{\partial q_{12}^{(2)}}{\partial \xi_2} \right) \right] \\ & + \left[N_{13}^{(2)} - \frac{4}{h_2^2} P_{13}^{(2)} \right] + \frac{1}{r^{(2)}} \left[M_{13}^{(2)} + M_{12}^{(2)} \cot \xi_2 - \frac{4}{3h_2^2} \left(q_{13}^{(2)} + q_{12}^{(2)} \cot \xi_2 \right) \right] + \frac{h_2}{3} \left[-\frac{N_{13}^{(1)}}{r^{(1)}} - \frac{N_{12}^{(1)}}{r^{(1)}} \cot \xi_2 + \frac{N_{13}^{(3)}}{r^{(3)}} + \frac{N_{12}^{(3)}}{r^{(3)}} \cot \xi_2 \right] \end{aligned} \right)$$

$$= \left\{ \begin{aligned} & \left(-\frac{h_2}{3} I_0^{(1)} + I_1^{(2)} - \frac{4}{3h_2^2} I_3^{(2)} + \frac{h_2}{3} I_0^{(3)} \right) \ddot{u}_0 + \frac{h_2}{3} \left(\frac{h_1}{3} I_0^{(1)} - I_1^{(1)} + \frac{4}{3h_2^2} I_3^{(1)} \right) \ddot{\psi}_1^{(1)} \\ & + \left(\frac{h_2^2}{9} \left(I_0^{(1)} + I_0^{(3)} \right) + I_2^{(2)} - \frac{8}{3h_2^2} I_4^{(2)} + \frac{16}{9h_2^4} I_6^{(2)} \right) \ddot{\psi}_1^{(2)} + \frac{h_2}{3} \left(\frac{h_3}{3} I_0^{(3)} + I_1^{(3)} - \frac{4}{3h_2^2} I_3^{(3)} \right) \ddot{\psi}_1^{(3)} \\ & + \frac{h_2}{3} \left(\frac{h_1^2}{8} I_0^{(1)} + \frac{1}{2} I_2^{(1)} \right) \ddot{\alpha}_1^{(1)} + \left(\frac{h_2^2}{24} \left(I_0^{(1)} - I_0^{(3)} \right) - \frac{1}{2} I_3^{(2)} + \frac{2}{3h_2^2} I_5^{(2)} \right) \ddot{\alpha}_1^{(2)} - \frac{h_2}{3} \left(\frac{h_2^3}{8} I_0^{(3)} + \frac{1}{2} I_2^{(3)} \right) \ddot{\alpha}_1^{(3)} \\ & - \frac{h_2}{3} \left(\frac{h_1^3}{24} I_0^{(1)} - \frac{1}{3} I_3^{(1)} \right) \ddot{\lambda}_1^{(1)} - \left(\frac{h_2^4}{72} \left(I_0^{(1)} + I_0^{(3)} \right) + \frac{1}{3} I_4^{(2)} - \frac{4}{9h_2^2} I_6^{(2)} \right) \ddot{\lambda}_1^{(2)} - \frac{h_2}{3} \left(\frac{h_3^3}{24} I_0^{(3)} + \frac{1}{3} I_3^{(3)} \right) \ddot{\lambda}_1^{(3)} \\ & + \frac{8h_2}{9h_1^2} I_0^{(1)} \ddot{\beta}_1^{(1)} + \frac{4}{3h_2^2} \left(\frac{h_2}{3} \left(I_0^{(1)} - I_0^{(3)} \right) - I_1^{(2)} + \frac{4}{3h_2^2} I_3^{(2)} \right) \ddot{\beta}_1^{(2)} - \frac{8h_2}{9h_2^3} I_0^{(3)} \ddot{\beta}_1^{(3)} \end{aligned} \right\} \quad (10c)$$

$$\delta \psi_1^{(3)} : \left(\begin{aligned} & \frac{h_3}{3r^{(3)}} \left[\frac{1}{\sin \xi_2} \frac{\partial N_{11}^{(3)}}{\partial \xi_1} + \frac{\partial N_{12}^{(3)}}{\partial \xi_2} \right] - \frac{1}{r^{(3)}} \left[\frac{1}{\sin \xi_2} \frac{\partial M_{11}^{(3)}}{\partial \xi_1} + \frac{\partial M_{12}^{(3)}}{\partial \xi_2} - \frac{4}{3h_3^2} \left(\frac{1}{\sin \xi_2} \frac{\partial q_{11}^{(3)}}{\partial \xi_1} + \frac{\partial q_{12}^{(3)}}{\partial \xi_2} \right) \right] \\ & + \left[\left(1 - \frac{h_3}{3r^{(3)}} \right) N_{13}^{(3)} - \frac{h_3}{3r^{(3)}} N_{12}^{(3)} \cot \xi_2 - \frac{4}{h_3^2} P_{13}^{(3)} \right] + \frac{1}{r^{(3)}} \left[M_{13}^{(3)} + M_{12}^{(3)} \cot \xi_2 - \frac{4}{3h_3^2} \left(q_{13}^{(3)} + q_{12}^{(3)} \cot \xi_2 \right) \right] \end{aligned} \right)$$

$$= \left\{ \begin{aligned} & \left(\frac{h_3}{3} I_0^{(3)} + I_1^{(3)} - \frac{4}{3h_2^2} I_3^{(3)} \right) \ddot{u}_0 + \frac{h_2}{3} \left(\frac{h_3}{3} I_0^{(3)} + I_1^{(3)} - \frac{4}{3h_2^2} I_3^{(3)} \right) \ddot{\psi}_1^{(2)} + \left(\frac{h_2^2}{9} I_0^{(3)} + \frac{2h_3}{3} I_1^{(3)} + I_2^{(3)} - \frac{8}{9h_3^3} I_3^{(3)} - \frac{8}{3h_2^2} I_4^{(3)} + \frac{16}{9h_3^4} I_6^{(3)} \right) \ddot{\psi}_1^{(3)} \\ & - \frac{h_2^2}{8} \left(\frac{h_3}{3} I_0^{(3)} + I_1^{(3)} - \frac{4}{3h_2^2} I_3^{(3)} \right) \ddot{\alpha}_1^{(2)} - \left(\frac{h_3^3}{24} I_0^{(3)} + \frac{h_3}{6} I_2^{(3)} + \frac{h_3^2}{8} I_1^{(3)} + \frac{1}{3} I_3^{(3)} + \frac{2}{3h_2^2} I_5^{(3)} \right) \ddot{\alpha}_1^{(3)} - \frac{h_2^3}{24} \left(\frac{h_3}{3} I_0^{(3)} + I_1^{(3)} - \frac{4}{3h_2^2} I_3^{(3)} \right) \ddot{\lambda}_1^{(2)} \\ & - \frac{1}{3} \left(\frac{h_3^4}{24} I_0^{(3)} + \frac{h_3^3}{8} I_1^{(3)} + \frac{h_3}{6} I_2^{(3)} + I_3^{(3)} - \frac{4}{3h_2^2} I_5^{(3)} \right) \ddot{\lambda}_1^{(3)} - \frac{4}{3h_2^2} \left(\frac{h_3}{3} I_0^{(3)} + I_1^{(3)} - \frac{4}{3h_2^2} I_3^{(3)} \right) \ddot{\beta}_1^{(2)} - \frac{8}{3h_2^2} \left(\frac{h_3}{3} I_0^{(3)} + I_1^{(3)} - \frac{4}{3h_2^2} I_3^{(3)} \right) \ddot{\beta}_1^{(3)} \end{aligned} \right\} \quad (10d)$$

$$\delta v_0 : \sum_{k=1}^3 \left(\frac{1}{r^{(k)}} \left[N_{11}^{(k)} \cot \xi_2 + \frac{\partial N_{22}^{(k)}}{\partial \xi_2} + \frac{1}{\sin \xi_2} \frac{\partial N_{12}^{(k)}}{\partial \xi_1} - N_{23}^{(k)} \right] \right)$$

$$= \left\{ \begin{aligned} & \left(I_0^{(1)} + I_0^{(2)} + I_0^{(3)} \right) \ddot{v}_0 + \left(-\frac{h_1}{3} + I_1^{(1)} - \frac{4}{3h_2^2} I_3^{(1)} \right) \ddot{\psi}_2^{(1)} + \left(-\frac{h_2}{3} I_0^{(1)} + I_1^{(2)} - \frac{4}{3h_2^2} I_3^{(2)} + \frac{h_2}{3} I_0^{(3)} \right) \ddot{\psi}_2^{(2)} + \left(\frac{h_3}{3} I_0^{(3)} + I_1^{(3)} - \frac{4}{3h_2^2} I_3^{(3)} \right) \ddot{\psi}_2^{(3)} \\ & - \left(\frac{h_1^2}{8} I_0^{(1)} + \frac{1}{2} I_2^{(1)} \right) \ddot{\alpha}_2^{(1)} - \left(\frac{h_2^2}{8} I_0^{(1)} + \frac{1}{2} I_2^{(2)} + \frac{h_2^2}{8} I_0^{(3)} \right) \ddot{\alpha}_2^{(2)} - \left(\frac{h_3^2}{8} I_0^{(3)} + \frac{1}{2} I_2^{(3)} \right) \ddot{\alpha}_2^{(3)} + \left(\frac{h_1^4}{24} I_0^{(1)} - \frac{1}{3} I_3^{(1)} \right) \ddot{\lambda}_2^{(1)} + \left(\frac{h_2^4}{24} I_0^{(1)} - \frac{1}{3} I_3^{(2)} - \frac{h_2^4}{24} I_0^{(3)} \right) \ddot{\lambda}_2^{(2)} \\ & - \left(\frac{h_3^4}{24} I_0^{(3)} + \frac{1}{3} I_3^{(3)} \right) \ddot{\lambda}_2^{(3)} - \frac{8}{3h_1^2} I_0^{(1)} \ddot{\beta}_2^{(1)} - \frac{4}{3h_2^2} \left(I_0^{(1)} + I_0^{(2)} + I_0^{(3)} \right) \ddot{\beta}_2^{(2)} - \frac{8}{3h_3^2} I_0^{(3)} \ddot{\beta}_2^{(3)} \end{aligned} \right\} \quad (10e)$$

$$\delta \psi_2^{(1)} : \left(-\frac{h_1}{3r^{(1)}} \left[\frac{1}{\sin \xi_2} \frac{\partial N_{12}^{(1)}}{\partial \xi_1} + \frac{\partial N_{22}^{(1)}}{\partial \xi_2} \right] - \frac{1}{r^{(1)}} \left[\frac{1}{\sin \xi_2} \frac{\partial M_{12}^{(1)}}{\partial \xi_1} + \frac{\partial M_{22}^{(1)}}{\partial \xi_2} - \frac{4}{3h_1^2} \left(\frac{1}{\sin \xi_2} \frac{\partial q_{12}^{(1)}}{\partial \xi_1} + \frac{\partial q_{22}^{(1)}}{\partial \xi_2} \right) \right] \right)$$

$$= \left(-\frac{h_1}{3r^{(1)}} N_{11}^{(1)} \cot \xi_2 + \left(1 + \frac{h_1}{3r^{(1)}} \right) N_{23}^{(1)} - \frac{4}{h_1^2} P_{23}^{(1)} - \frac{1}{r^{(1)}} \left[M_{11}^{(1)} \cot \xi_2 - M_{23}^{(1)} - \frac{4}{3h_1^2} \left(q_{11}^{(1)} \cot \xi_2 - q_{23}^{(1)} \right) \right] \right)$$

$$= \left\{ \begin{aligned} & \left(-\frac{h_1}{3} I_0^{(1)} + I_1^{(1)} - \frac{4}{3h_2^2} I_3^{(1)} \right) \ddot{v}_0 + \left(\frac{h_2^2}{9} I_0^{(1)} - \frac{2h_1}{3} I_1^{(1)} + I_2^{(1)} + \frac{8}{9h_1^3} I_3^{(1)} - \frac{8}{3h_2^2} I_4^{(1)} + \frac{16}{9h_1^4} I_6^{(1)} \right) \ddot{\psi}_2^{(1)} - \frac{h_2}{3} \left(-\frac{h_1}{3} I_0^{(1)} + I_1^{(1)} - \frac{4}{3h_2^2} I_3^{(1)} \right) \ddot{\psi}_2^{(2)} \\ & + \left(\frac{h_1^3}{24} I_0^{(1)} - \frac{h_1^2}{8} I_1^{(1)} + \frac{h_1}{6} I_2^{(1)} - \frac{1}{3} I_3^{(1)} + \frac{2}{3h_1^2} I_5^{(1)} \right) \ddot{\alpha}_2^{(1)} - \frac{h_2^2}{8} \left(-\frac{h_1}{3} I_0^{(1)} + I_1^{(1)} - \frac{4}{3h_2^2} I_3^{(1)} \right) \ddot{\alpha}_2^{(2)} + \frac{1}{3} \left(-\frac{h_1^4}{24} I_0^{(1)} + \frac{h_1^3}{8} I_1^{(1)} + \frac{h_1}{6} I_2^{(1)} - I_3^{(1)} + \frac{4}{3h_1^2} I_5^{(1)} \right) \ddot{\lambda}_2^{(1)} \\ & + \frac{h_2^2}{24} \left(-\frac{h_1}{3} I_0^{(1)} + I_1^{(1)} - \frac{4}{3h_2^2} I_3^{(1)} \right) \ddot{\lambda}_2^{(2)} - \frac{8}{3h_1^2} \left(-\frac{h_1}{3} I_0^{(1)} + I_1^{(1)} - \frac{4}{3h_2^2} I_3^{(1)} \right) \ddot{\beta}_2^{(1)} - \frac{4}{3h_2^2} \left(-\frac{h_1}{3} I_0^{(1)} + I_1^{(1)} - \frac{4}{3h_2^2} I_3^{(1)} \right) \ddot{\beta}_2^{(2)} \end{aligned} \right\} \quad (10f)$$

$$\delta \psi_2^{(2)} : \left(\frac{h_2}{3 \sin \xi_2} \left[\frac{1}{r^{(1)}} \frac{\partial N_{12}^{(1)}}{\partial \xi_1} - \frac{1}{r^{(3)}} \frac{\partial N_{12}^{(3)}}{\partial \xi_1} \right] + \frac{h_2}{3} \left[\frac{1}{r^{(1)}} \frac{\partial N_{22}^{(1)}}{\partial \xi_2} - \frac{1}{r^{(3)}} \frac{\partial N_{22}^{(3)}}{\partial \xi_2} \right] - \frac{1}{r^{(2)}} \left[\frac{1}{\sin \xi_2} \frac{\partial M_{12}^{(2)}}{\partial \xi_1} + \frac{\partial M_{22}^{(2)}}{\partial \xi_2} - \frac{4}{3h_2^2} \left(\frac{1}{\sin \xi_2} \frac{\partial q_{12}^{(2)}}{\partial \xi_1} + \frac{\partial q_{22}^{(2)}}{\partial \xi_2} \right) \right] \right)$$

$$= \left(-\frac{1}{r^{(2)}} \left[M_{11}^{(2)} \cot \xi_2 + M_{23}^{(2)} - \frac{4}{3h_2^2} \left(q_{11}^{(2)} \cot \xi_2 + q_{23}^{(2)} \right) \right] + \left[N_{23}^{(2)} - \frac{4}{h_2^2} P_{23}^{(2)} \right] + \frac{h_2}{3} \left[\frac{N_{11}^{(1)}}{r^{(1)}} \cot \xi_2 - \frac{N_{23}^{(1)}}{r^{(1)}} - \frac{N_{11}^{(3)}}{r^{(3)}} \cot \xi_2 + \frac{N_{23}^{(3)}}{r^{(3)}} \right] \right)$$

$$= \left\{ \begin{aligned} & \left(-\frac{h_2}{3} I_0^{(1)} + I_1^{(2)} - \frac{4}{3h_2^2} I_3^{(2)} + \frac{h_2}{3} I_0^{(3)} \right) \ddot{v}_0 + \frac{h_2}{3} \left(\frac{h_1}{3} I_0^{(1)} - I_1^{(1)} + \frac{4}{3h_2^2} I_3^{(1)} \right) \ddot{\psi}_2^{(1)} \\ & + \left(\frac{h_2^2}{9} \left(I_0^{(1)} + I_0^{(3)} \right) + I_2^{(2)} - \frac{8}{3h_2^2} I_4^{(2)} + \frac{16}{9h_2^4} I_6^{(2)} \right) \ddot{\psi}_2^{(2)} + \frac{h_2}{3} \left(\frac{h_3}{3} I_0^{(3)} + I_1^{(3)} - \frac{4}{3h_2^2} I_3^{(3)} \right) \ddot{\psi}_2^{(3)} \\ & + \frac{h_2}{3} \left(\frac{h_1^2}{8} I_0^{(1)} + \frac{1}{2} I_2^{(1)} \right) \ddot{\alpha}_2^{(1)} + \left(\frac{h_2^2}{24} \left(I_0^{(1)} - I_0^{(3)} \right) - \frac{1}{2} I_3^{(2)} + \frac{2}{3h_2^2} I_5^{(2)} \right) \ddot{\alpha}_2^{(2)} - \frac{h_2}{3} \left(\frac{h_3^2}{8} I_0^{(3)} + \frac{1}{2} I_2^{(3)} \right) \ddot{\alpha}_2^{(3)} \\ & - \frac{h_2}{3} \left(\frac{h_1^3}{24} I_0^{(1)} - \frac{1}{3} I_3^{(1)} \right) \ddot{\lambda}_2^{(1)} - \left(\frac{h_2^4}{72} \left(I_0^{(1)} + I_0^{(3)} \right) + \frac{1}{3} I_4^{(2)} - \frac{4}{9h_2^2} I_6^{(2)} \right) \ddot{\lambda}_2^{(2)} - \frac{h_2}{3} \left(\frac{h_3^3}{24} I_0^{(3)} + \frac{1}{3} I_3^{(3)} \right) \ddot{\lambda}_2^{(3)} \\ & + \frac{8h_2}{9h_1^2} I_0^{(1)} \ddot{\beta}_2^{(1)} + \frac{4}{3h_2^2} \left(\frac{h_2}{3} \left(I_0^{(1)} - I_0^{(3)} \right) - I_1^{(2)} + \frac{4}{3h_2^2} I_3^{(2)} \right) \ddot{\beta}_2^{(2)} - \frac{8h_2}{9h_3^2} I_0^{(3)} \ddot{\beta}_2^{(3)} \end{aligned} \right\} \quad (10g)$$

$$\delta \psi_2^{(3)} : \left(\frac{h_3}{3r^{(3)}} \left[\frac{1}{\sin \xi_2} \frac{\partial N_{12}^{(3)}}{\partial \xi_1} + \frac{\partial N_{22}^{(3)}}{\partial \xi_2} \right] - \frac{1}{r^{(3)}} \left[\frac{1}{\sin \xi_2} \frac{\partial M_{12}^{(3)}}{\partial \xi_1} + \frac{\partial M_{22}^{(3)}}{\partial \xi_2} - \frac{4}{3h_3^2} \left(\frac{1}{\sin \xi_2} \frac{\partial q_{12}^{(3)}}{\partial \xi_1} + \frac{\partial q_{22}^{(3)}}{\partial \xi_2} \right) \right] \right)$$

$$= \left(\frac{h_3}{3r^{(3)}} N_{11}^{(3)} \cot \xi_2 + \left(1 - \frac{h_3}{3r^{(3)}} \right) N_{23}^{(3)} - \frac{4}{h_3^2} P_{23}^{(3)} - \frac{1}{r^{(3)}} \left[M_{11}^{(3)} \cot \xi_2 - M_{23}^{(3)} - \frac{4}{3h_3^2} \left(q_{11}^{(3)} \cot \xi_2 - q_{23}^{(3)} \right) \right] \right)$$

$$= \left\{ \begin{aligned} & \left(\frac{h_3}{3} I_0^{(3)} + I_1^{(3)} - \frac{4}{3h_2^2} I_3^{(3)} \right) \ddot{v}_0 + \frac{h_2}{3} \left(\frac{h_3}{3} I_0^{(3)} + I_1^{(3)} - \frac{4}{3h_2^2} I_3^{(3)} \right) \ddot{\psi}_2^{(2)} + \left(\frac{h_2^2}{9} I_0^{(3)} + \frac{2h_2}{3} I_1^{(3)} + I_2^{(2)} - \frac{8}{9h_2^3} I_3^{(3)} - \frac{8}{3h_2^2} I_4^{(2)} + \frac{16}{9h_2^4} I_6^{(2)} \right) \ddot{\psi}_2^{(3)} \\ & - \frac{h_2^2}{8} \left(\frac{h_3}{3} I_0^{(3)} + I_1^{(3)} - \frac{4}{3h_2^2} I_3^{(3)} \right) \ddot{\alpha}_2^{(2)} - \left(\frac{h_3^3}{24} I_0^{(3)} + \frac{h_2^2}{8} I_1^{(3)} + \frac{h_2}{6} I_2^{(2)} + \frac{1}{3} I_3^{(3)} - \frac{2}{3h_2^2} I_5^{(3)} \right) \ddot{\alpha}_2^{(3)} - \frac{h_2^3}{24} \left(\frac{h_3}{3} I_0^{(3)} + I_1^{(3)} - \frac{4}{3h_2^2} I_3^{(3)} \right) \ddot{\lambda}_2^{(2)} \\ & - \frac{1}{3} \left(\frac{h_3^4}{24} I_0^{(3)} + \frac{h_2^3}{8} I_1^{(3)} + \frac{h_2}{6} I_2^{(2)} + I_3^{(3)} - \frac{4}{3h_2^2} I_5^{(3)} \right) \ddot{\lambda}_2^{(3)} - \frac{4}{3h_2^2} \left(\frac{h_3}{3} I_0^{(3)} + I_1^{(3)} - \frac{4}{3h_2^2} I_3^{(3)} \right) \ddot{\beta}_2^{(2)} - \frac{8}{3h_2^2} \left(\frac{h_3}{3} I_0^{(3)} + I_1^{(3)} - \frac{4}{3h_2^2} I_3^{(3)} \right) \ddot{\beta}_2^{(3)} \end{aligned} \right\} \quad (10h)$$

$$\delta w_0 : \sum_{k=1}^3 \left(\frac{1}{r^{(k)}} \left[N_{11}^{(k)} + N_{22}^{(k)} + \frac{\partial N_{23}^{(k)}}{\partial \xi_2} + \frac{1}{\sin \xi_2} \frac{\partial N_{13}^{(k)}}{\partial \xi_1} \right] \right)$$

$$= \left\{ \begin{aligned} & \left(I_0^{(1)} + I_0^{(2)} + I_0^{(3)} \right) \ddot{w}_0 + \left(-\frac{h_1}{2} I_0^{(1)} + I_1^{(1)} \right) \ddot{\psi}_3^{(1)} + \left(-\frac{h_2}{2} I_0^{(1)} + I_1^{(2)} + \frac{h_2}{2} I_0^{(3)} \right) \ddot{\psi}_3^{(2)} \\ & + \left(\frac{h_3}{2} I_0^{(3)} + I_1^{(3)} \right) \ddot{\psi}_3^{(3)} + \left(\frac{h_1^2}{4} I_0^{(1)} + I_2^{(1)} \right) \ddot{\alpha}_3^{(1)} + \left(\frac{h_2^2}{4} I_0^{(1)} + I_2^{(2)} \right) \ddot{\alpha}_3^{(2)} + \left(\frac{h_3^2}{4} I_0^{(3)} + I_2^{(3)} \right) \ddot{\alpha}_3^{(3)} \end{aligned} \right\} + \frac{2\pi}{3} P_0 a_{\max}^2 \sin \left(\frac{\pi t}{t_{\max}} \right) \quad (10i)$$

$$\delta\psi_3^{(1)} : \left(-\frac{h_1}{2r^{(1)}} \left[\frac{1}{\sin \xi_2} \frac{\partial N_{13}^{(1)}}{\partial \xi_1} + \frac{\partial N_{23}^{(1)}}{\partial \xi_2} + N_{11}^{(1)} + N_{22}^{(1)} \right] - \frac{1}{r^{(1)}} \left[\frac{1}{\sin \xi_2} \frac{\partial M_{13}^{(1)}}{\partial \xi_1} + \frac{\partial M_{23}^{(1)}}{\partial \xi_2} + M_{11}^{(1)} + M_{22}^{(1)} \right] + N_{33}^{(1)} \right) \\ = \left\{ \begin{aligned} & \left(-\frac{h_1}{2} I_0^{(1)} + I_1^{(1)} \right) \ddot{w}_0 + \left(\frac{h_1^2}{4} I_0^{(1)} - h_1 I_1^{(1)} + I_2^{(1)} \right) \ddot{\psi}_3^{(1)} - \frac{h_2}{2} \left(-\frac{h_1}{2} I_0^{(1)} + I_1^{(1)} \right) \ddot{\psi}_3^{(2)} \\ & + \left(-\frac{h_1^3}{8} I_0^{(1)} + \frac{h_1^2}{4} I_1^{(1)} - \frac{h_1}{2} I_2^{(1)} + I_3^{(1)} \right) \ddot{\alpha}_3^{(1)} + \frac{h_2^2}{4} \left(-\frac{h_1}{2} I_0^{(1)} + I_1^{(1)} \right) \ddot{\alpha}_3^{(2)} \end{aligned} \right\} \tag{10j}$$

$$\delta\psi_3^{(2)} : \left(\frac{h_2}{2} \left[\frac{1}{r^{(1)}} \left(\frac{1}{\sin \xi_2} \frac{\partial N_{13}^{(1)}}{\partial \xi_1} + \frac{\partial N_{23}^{(1)}}{\partial \xi_2} \right) - \frac{1}{r^{(3)}} \left(\frac{1}{\sin \xi_2} \frac{\partial N_{13}^{(3)}}{\partial \xi_1} + \frac{\partial N_{23}^{(3)}}{\partial \xi_2} \right) \right] - \frac{1}{r^{(2)}} \left[\frac{1}{\sin \xi_2} \frac{\partial M_{13}^{(2)}}{\partial \xi_1} + \frac{\partial M_{23}^{(2)}}{\partial \xi_2} \right] \right) \\ + \frac{h_2}{2} \left[\frac{N_{11}^{(1)}}{r^{(1)}} + \frac{N_{22}^{(1)}}{r^{(1)}} - \frac{N_{11}^{(3)}}{r^{(3)}} - \frac{N_{22}^{(3)}}{r^{(3)}} \right] - \frac{1}{r^{(2)}} \left[M_{11}^{(2)} + M_{22}^{(2)} \right] + N_{33}^{(2)} \\ = \left\{ \begin{aligned} & \left(-\frac{h_2}{2} I_0^{(1)} + I_1^{(2)} + \frac{h_2}{2} I_0^{(3)} \right) \ddot{w}_0 + \frac{h_2}{2} \left(\frac{h_1}{2} I_0^{(1)} - I_1^{(1)} \right) \ddot{\psi}_3^{(1)} \\ & + \left(\frac{h_2^2}{4} \left(I_0^{(1)} + I_0^{(3)} \right) + I_2^{(2)} \right) \ddot{\psi}_3^{(2)} + \frac{h_2}{2} \left(\frac{h_2}{2} I_0^{(3)} + I_1^{(3)} \right) \ddot{\psi}_3^{(3)} - \frac{h_2}{2} \left(\frac{h_1^2}{4} I_0^{(1)} + I_2^{(1)} \right) \ddot{\alpha}_3^{(1)} \\ & + \left(\frac{h_2^3}{8} \left(-I_0^{(1)} + I_0^{(3)} \right) + I_3^{(2)} \right) \ddot{\alpha}_3^{(2)} + \frac{h_2}{2} \left(\frac{h_2^2}{4} I_0^{(3)} + I_2^{(3)} \right) \ddot{\alpha}_3^{(3)} \end{aligned} \right\} + \frac{\pi h_2}{3} P_0 a_{\max}^2 \sin \left(\frac{\pi t}{t_{\max}} \right) \tag{10k}$$

$$\delta\psi_3^{(3)} : \left(\frac{h_3}{2r^{(3)}} \left[\frac{1}{\sin \xi_2} \frac{\partial N_{13}^{(3)}}{\partial \xi_1} + \frac{\partial N_{23}^{(3)}}{\partial \xi_2} + N_{11}^{(3)} + N_{22}^{(3)} \right] - \frac{1}{r^{(3)}} \left[\frac{1}{\sin \xi_2} \frac{\partial M_{13}^{(3)}}{\partial \xi_1} + \frac{\partial M_{23}^{(3)}}{\partial \xi_2} + M_{11}^{(3)} + M_{22}^{(3)} \right] + N_{33}^{(3)} \right) \\ = \left\{ \begin{aligned} & \left(\frac{h_3}{2} I_0^{(3)} + I_1^{(3)} \right) \ddot{w}_0 + \frac{h_2}{2} \left(\frac{h_2}{2} I_0^{(3)} + I_1^{(3)} \right) \ddot{\psi}_3^{(2)} + \left(\frac{h_3^2}{4} I_0^{(3)} + h_3 I_1^{(3)} + I_2^{(3)} \right) \ddot{\psi}_3^{(3)} \\ & + \frac{h_2^2}{4} \left(\frac{h_3}{2} I_0^{(3)} + I_1^{(3)} \right) \ddot{\alpha}_3^{(2)} + \left(\frac{h_3^3}{8} I_0^{(3)} + \frac{h_3^2}{4} I_1^{(3)} + \frac{h_3}{2} I_2^{(3)} + I_3^{(3)} \right) \ddot{\alpha}_3^{(3)} \end{aligned} \right\} + \frac{2\pi h_3}{3} P_0 a_{\max}^2 \sin \left(\frac{\pi t}{t_{\max}} \right) \tag{10l}$$

$$\delta\alpha_3^{(1)} : \left(\frac{h_1^2}{4r^{(1)}} \left[\frac{1}{\sin \xi_2} \frac{\partial N_{13}^{(1)}}{\partial \xi_1} + \frac{\partial N_{23}^{(1)}}{\partial \xi_2} + N_{11}^{(1)} + N_{22}^{(1)} \right] + \frac{1}{r^{(1)}} \left[\frac{1}{\sin \xi_2} \frac{\partial P_{13}^{(1)}}{\partial \xi_1} + \frac{\partial P_{23}^{(1)}}{\partial \xi_2} + P_{11}^{(1)} + P_{22}^{(1)} \right] - 2M_{33}^{(1)} \right) \\ = \left\{ \begin{aligned} & \left(\frac{h_1^2}{4} I_0^{(1)} + I_2^{(1)} \right) \ddot{w}_0 + \left(-\frac{h_1^3}{8} I_0^{(1)} + \frac{h_1^2}{4} I_1^{(1)} - \frac{h_1}{2} I_2^{(1)} + I_3^{(1)} \right) \ddot{\psi}_3^{(1)} - \frac{h_2}{2} \left(\frac{h_1^2}{4} I_0^{(1)} + I_2^{(1)} \right) \ddot{\psi}_3^{(2)} \\ & + \left(\frac{h_1^4}{16} I_0^{(1)} + \frac{h_1^2}{2} I_2^{(1)} + I_4^{(1)} \right) \ddot{\alpha}_3^{(1)} + \frac{h_2^2}{4} \left(\frac{h_1^2}{4} I_0^{(1)} + I_2^{(1)} \right) \ddot{\alpha}_3^{(2)} \end{aligned} \right\} \tag{10m}$$

$$\delta\alpha_3^{(2)} : \left(\frac{1}{r^{(2)}} \left[\frac{1}{\sin \xi_2} \frac{\partial P_{13}^{(2)}}{\partial \xi_1} + \frac{\partial P_{23}^{(2)}}{\partial \xi_2} + P_{11}^{(2)} + P_{22}^{(2)} \right] - \frac{h_2^2}{4} \left[\frac{1}{r^{(1)}} \left(\frac{1}{\sin \xi_2} \frac{\partial N_{13}^{(1)}}{\partial \xi_1} + \frac{\partial N_{23}^{(1)}}{\partial \xi_2} + N_{11}^{(1)} + N_{22}^{(1)} \right) + \frac{1}{r^{(3)}} \left(\frac{1}{\sin \xi_2} \frac{\partial N_{13}^{(3)}}{\partial \xi_1} + \frac{\partial N_{23}^{(3)}}{\partial \xi_2} + N_{11}^{(3)} + N_{22}^{(3)} \right) \right] - 2M_{33}^{(2)} \right) \\ = \left\{ \begin{aligned} & \left(\frac{h_2^2}{4} \left(I_0^{(1)} + I_0^{(3)} \right) + I_2^{(2)} \right) \ddot{w}_0 + \frac{h_2}{4} \left(-\frac{h_1}{2} I_0^{(1)} + I_1^{(1)} \right) \ddot{\psi}_3^{(1)} + \left(\frac{h_2^3}{8} \left(-I_0^{(1)} + I_0^{(3)} \right) + I_3^{(2)} \right) \ddot{\psi}_3^{(2)} \\ & + \frac{h_2^2}{4} \left(\frac{h_2}{2} I_0^{(3)} + I_1^{(3)} \right) \ddot{\psi}_3^{(3)} + \frac{h_2^2}{4} \left(\frac{h_2^2}{4} I_0^{(1)} + I_2^{(1)} \right) \ddot{\alpha}_3^{(1)} + \left(\frac{h_2^2}{4} \left(I_0^{(1)} + I_0^{(3)} \right) + I_4^{(2)} \right) \ddot{\alpha}_3^{(2)} \\ & + \frac{h_2^2}{4} \left(\frac{h_2^3}{4} I_0^{(3)} + I_2^{(3)} \right) \ddot{\alpha}_3^{(3)} \end{aligned} \right\} + \frac{\pi h_2^2}{6} P_0 a_{\max}^2 \sin \left(\frac{\pi t}{t_{\max}} \right) \tag{10n}$$

$$\delta\alpha_3^{(3)} : \left(\frac{h_3^2}{4r^{(3)}} \left[\frac{1}{\sin \xi_2} \frac{\partial N_{13}^{(3)}}{\partial \xi_1} + \frac{\partial N_{23}^{(3)}}{\partial \xi_2} + N_{11}^{(3)} + N_{22}^{(3)} \right] + \frac{1}{r^{(3)}} \left[\frac{1}{\sin \xi_2} \frac{\partial P_{13}^{(3)}}{\partial \xi_1} + \frac{\partial P_{23}^{(3)}}{\partial \xi_2} + P_{11}^{(3)} + P_{22}^{(3)} \right] - 2M_{33}^{(3)} \right) \\ = \left\{ \begin{aligned} & \left(\frac{h_3^2}{4} I_0^{(3)} + I_2^{(3)} \right) \ddot{w}_0 + \frac{h_2}{2} \left(\frac{h_2^2}{4} I_0^{(3)} + I_2^{(3)} \right) \ddot{\psi}_3^{(2)} + \left(\frac{h_3^3}{8} I_0^{(3)} + \frac{h_3}{2} I_2^{(3)} + \frac{h_2^2}{4} I_1^{(3)} + I_3^{(3)} \right) \ddot{\psi}_3^{(3)} \\ & + \frac{h_2^2}{4} \left(\frac{h_3^2}{4} I_0^{(3)} + I_2^{(3)} \right) \ddot{\alpha}_3^{(2)} + \left(\frac{h_3^4}{16} I_0^{(3)} + \frac{h_3^2}{4} I_2^{(3)} + \frac{h_3}{4} I_3^{(3)} + I_4^{(3)} \right) \ddot{\alpha}_3^{(3)} \end{aligned} \right\} + \frac{\pi h_3^2}{3} P_0 a_{\max}^2 \sin \left(\frac{\pi t}{t_{\max}} \right) \tag{10o}$$

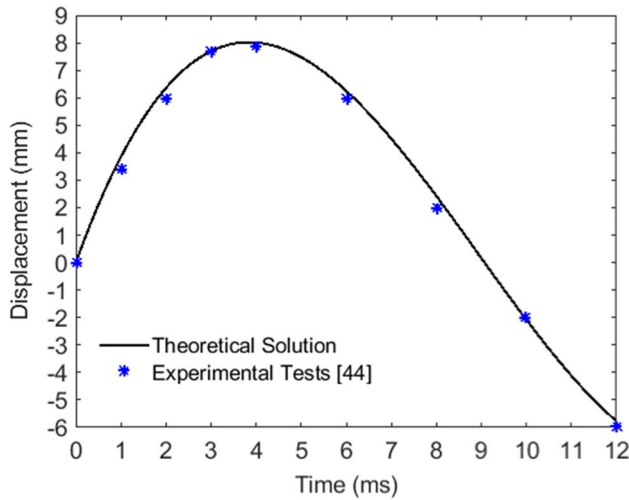


Fig. 4 The variation of displacement in terms of time in the composite plate subjected to a hemispherical projectile with an initial velocity of 4 m/s

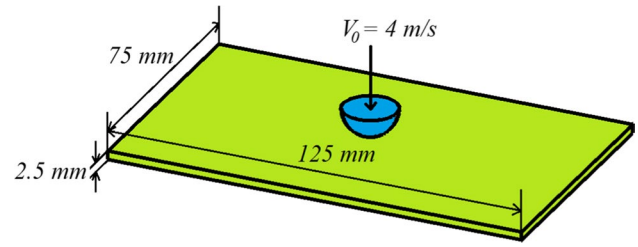


Fig. 3 The rectangular composite laminated plate with ply-angle [0/45/45/90]_s subjected to the low-velocity impact of a hemispherical projectile with an initial velocity of 4 m/s

$$\delta\varphi^{(1)} : \frac{1}{\sin \xi_2} \frac{\partial \Gamma_1^{(1)}}{\partial \xi_1} + \frac{\partial \Gamma_2^{(1)}}{\partial \xi_1} - \Gamma_3^{(1)} = 0 \quad (10p)$$

$$\delta\varphi^{(3)} : \frac{1}{\sin \xi_2} \frac{\partial \Gamma_1^{(3)}}{\partial \xi_1} + \frac{\partial \Gamma_2^{(3)}}{\partial \xi_1} - \Gamma_3^{(3)} = 0 \quad (10q)$$

In order to satisfy Maxwell's static equation, Eqs. (11a) and (11b) need to be true for the first and third piezoelectric face sheets of the spherical sandwich shell, respectively.

$$\vec{\nabla} \cdot \vec{D}^{(1)} = 0 \Rightarrow \frac{1}{r^{(1)} \sin \xi_2} \frac{\partial D_1^{(1)}}{\partial \xi_1} + \frac{1}{r^{(1)} \sin \xi_2} \frac{\partial (D_2^{(1)} \sin \xi_2)}{\partial \xi_2} + \frac{\partial D_3^{(1)}}{\partial \xi} + \frac{2D_3^{(1)}}{r^{(1)}} = 0 \quad (11a)$$

$$\vec{\nabla} \cdot \vec{D}^{(3)} = 0 \Rightarrow \frac{1}{r^{(3)} \sin \xi_2} \frac{\partial D_1^{(3)}}{\partial \xi_1} + \frac{1}{r^{(3)} \sin \xi_2} \frac{\partial (D_2^{(3)} \sin \xi_2)}{\partial \xi_2} + \frac{\partial D_3^{(3)}}{\partial \xi} + \frac{2D_3^{(3)}}{r^{(3)}} = 0 \quad (11b)$$

By inserting Eqs. (C1)–(C13) and (D3) into Eqs. (11) and classifying relations, Eqs. (12) can be written. In order to solve the low-velocity impact problem in the spherical

sandwich shell, it is necessary that the nineteen Eqs. (10) and (12) are solved together.

Table 1 The mechanical properties of the composite carbon fiber/epoxy laminated plate [44]

E_1 (GPa)	E_2 (GPa)	E_3 (GPa)	ν_{12}	G_{12} (GPa)	G_{23} (GPa)	ρ (Kg/m ³)
55	4	4	0.3	1.35	1.35	1600

Table 2 The geometrical location of two points defined in Fig. 1 on the spherical coordinate system

Point number	Location on the	ξ -Coordinate	ξ_1 -Coordinate	ξ_2 -Coordinate
Point 1	Top piezoelectric layer	$R + h/2$	$\pi/2$	0
Point 2	FG-CNT core	$R + h/2$	$\pi/2$	$a_{\max}/(R + h/2)$

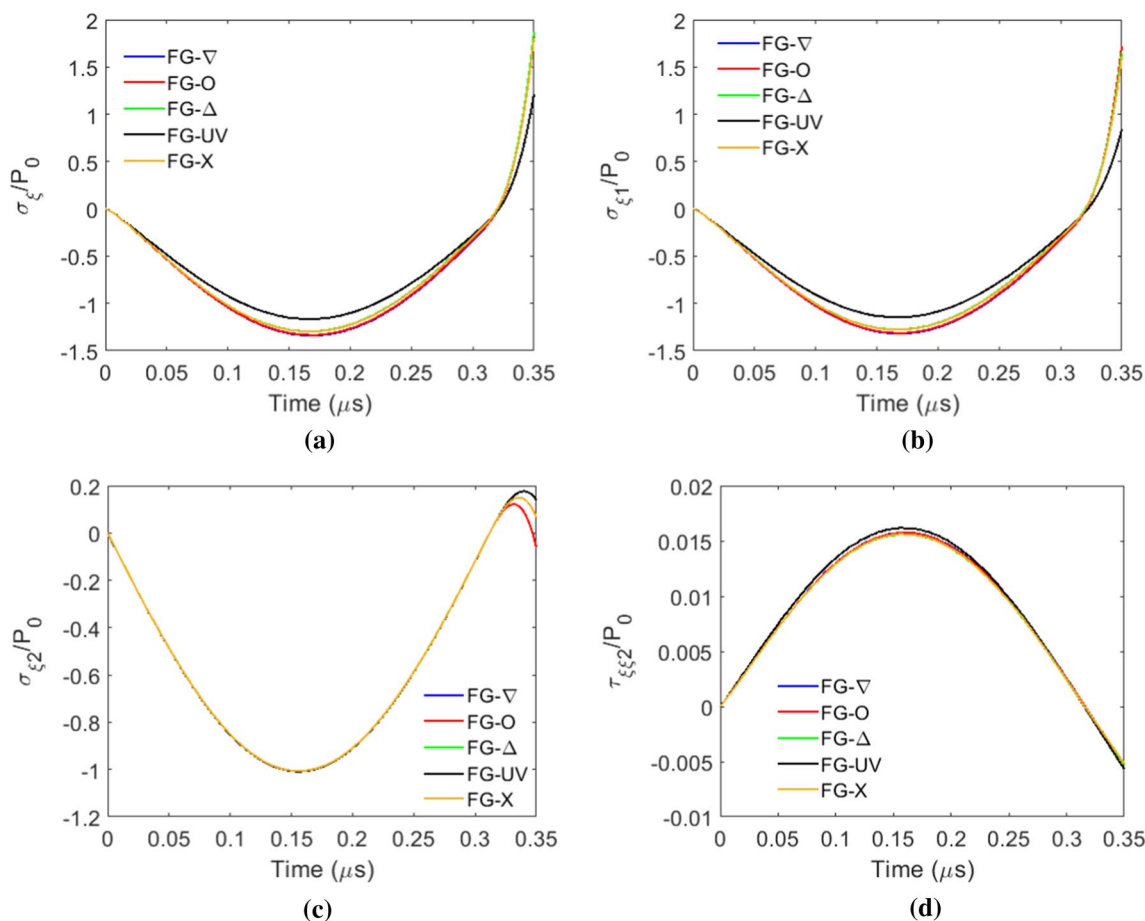


Fig. 5 The variation of the stress components in terms of time, **a** σ_{ξ_2} at point 1, **b** σ_{ξ_1} at point 1, **c** σ_{ξ_3} at point 1, **d** $\tau_{\xi_1\xi_2}$ at point 2, for $h/R = 0.1, h_1/h = 0.1, R = 5 \text{ mm}$ and $\chi_0 = 30^\circ$

The spherical coordinates of two points, as well as the six paths that are highlighted in Fig. 1, are presented in the spherical coordinate system shown in Tables 2 and 3, respectively. The mechanical properties of the three layers of the spherical sandwich shell and spherical ball are presented in Table 4.

Figure 5 shows the stress distribution in terms of time in points 1 and 2 for the five samples as FG-UV, FG-∇, FG-Δ, FG-O, and FG-X. Figure 5a–c shows the variation of the radial stress (σ_{ξ_2}), the circumferential stress (σ_{ξ_1}), and the meridian stress (σ_{ξ_3}) in terms of time at point 1, respectively. Whereas, Fig. 5d shows the variation of the shear stress ($\tau_{\xi_1\xi_2}$) in terms of time at point 2. The shear stress is shown only at point 2 due to the fact that the maximum shear stress at this point causes on the top face sheet.

According to Fig. 5, it is observed that, the mechanical properties of the core have more effect on the stress components in the top face sheets. Moreover, it can be seen that the sector with FG-UV and FG-O has the minimum and maximum stress distribution in point 1. This means that when

the nanotubes are located in the center of the core relative to when they are made uniform leads to an increase in the stress distribution in the top face sheet. According to Fig. 5d, it can be seen that this nanotube arrangement has the opposite effect on shear stress.

Figure 6 shows the stress distribution in the outermost layer of the top piezoelectric face sheet (path 1) at $t = t_{\max}/2$, where the maximum stresses are observed in the sandwich shell. As shown in Fig. 6a–c, the maximum radial, circumferential, and meridian stresses are observed at the angle $\xi_2 = 0^\circ$ in the outermost layer of the top face sheet. According to Fig. 6d, the maximum shear stress occurs at the maximum radius of the contact area ($r = a_{\max}$ or $\xi_2 = a_{\max}/(R + h/2)$). According to Fig. 6a–c, it can be seen that the radial, circumferential, and meridian stresses are maximum in the sample FG-O as well as being minimum in the sample FG-UV. According to Fig. 6d, it can be seen that the shear stress has the maximum and minimum value in the samples FG-UV and FG-O, respectively.

Figure 7 shows the stress distribution in the innermost layer of the top piezoelectric face sheet (path 2) at $t = t_{\max}/2$,

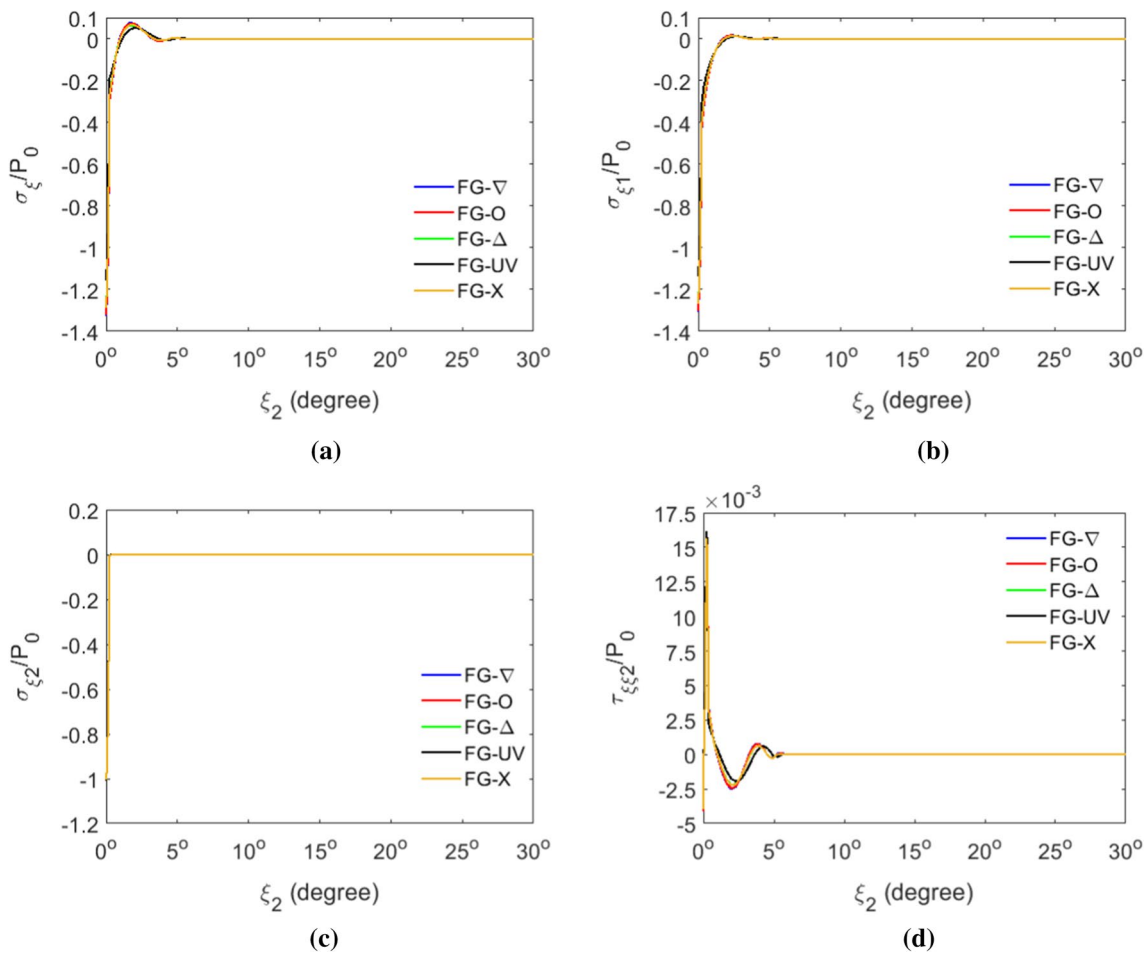


Fig. 6 The variation of the stress components in terms of ξ_2 on path 1, **a** σ_ξ , **b** σ_{ξ_1} , **c** σ_{ξ_2} , **d** $\tau_{\xi\xi_2}$, for $h/R = 0.1$, $h_1/h = 0.1$, $R = 5$ mm and $\chi_0 = 30^\circ$

where the maximum stresses are observed in the sandwich shell. As shown in Fig. 7, the maximum radial, circumferential and meridian stresses are generated at the angle $\xi_2 = 0$ in the innermost layer of the top face sheet. In addition, the maximum shear stress occurs at the maximum radius of the contact area ($r = a_{max}$ or $\xi_2 = a_{max}/(R + h/2)$). According to Fig. 4a, b, it can be seen that the radial and circumferential stresses are maximum in the sample FG-∇ as well as being minimum in the sample FG-UV. This means that when the nanotubes are located in the top layer of the core relative to when they are made uniform leads to an increase in the radial and circumferential stresses in the innermost layer of the top face sheet.

In addition, according to Fig. 7c, d, the meridian and shear stresses are maximum in the sample FG-Δ as well as being minimum in the sample FG-∇. This means that when the nanotubes are located in the bottom and top layers of the core, the maximum and minimum in both the meridian and shear stresses in the innermost layer of the top face sheet are generated, respectively.

Figure 8 shows the stress distribution in the outermost layer of the core (path 2) at $t = t_{max}/2$. As shown in Fig. 8, the maximum radial, circumferential, and shear stresses are generated at the angle $\xi_2 = a_{max}/(R + h/2)$. In addition, the maximum meridian stress occurs at the angle $\xi_2 = 0$. According to Fig. 8a, it can be seen that the radial stress has the maximum and minimum value in the samples FG-O and FG-UV, respectively. This means that when the nanotubes are located in the center of the core relative to when they are made uniform leads to an increase in the radial stress in the core.

According to Fig. 8b, d, it can be seen that the circumferential and shear stresses are maximum in the sample FG-Δ as well as being minimum in the sample FG-∇. This means that when the nanotubes are located in the bottom and top layers of the core, the maximum and minimum in both the circumferential and shear stresses in the core are generated, respectively.

According to Fig. 8c, it can be seen that the meridian stress has the maximum and minimum value in the samples FG-Δ and FG-UV, respectively. This means that when the

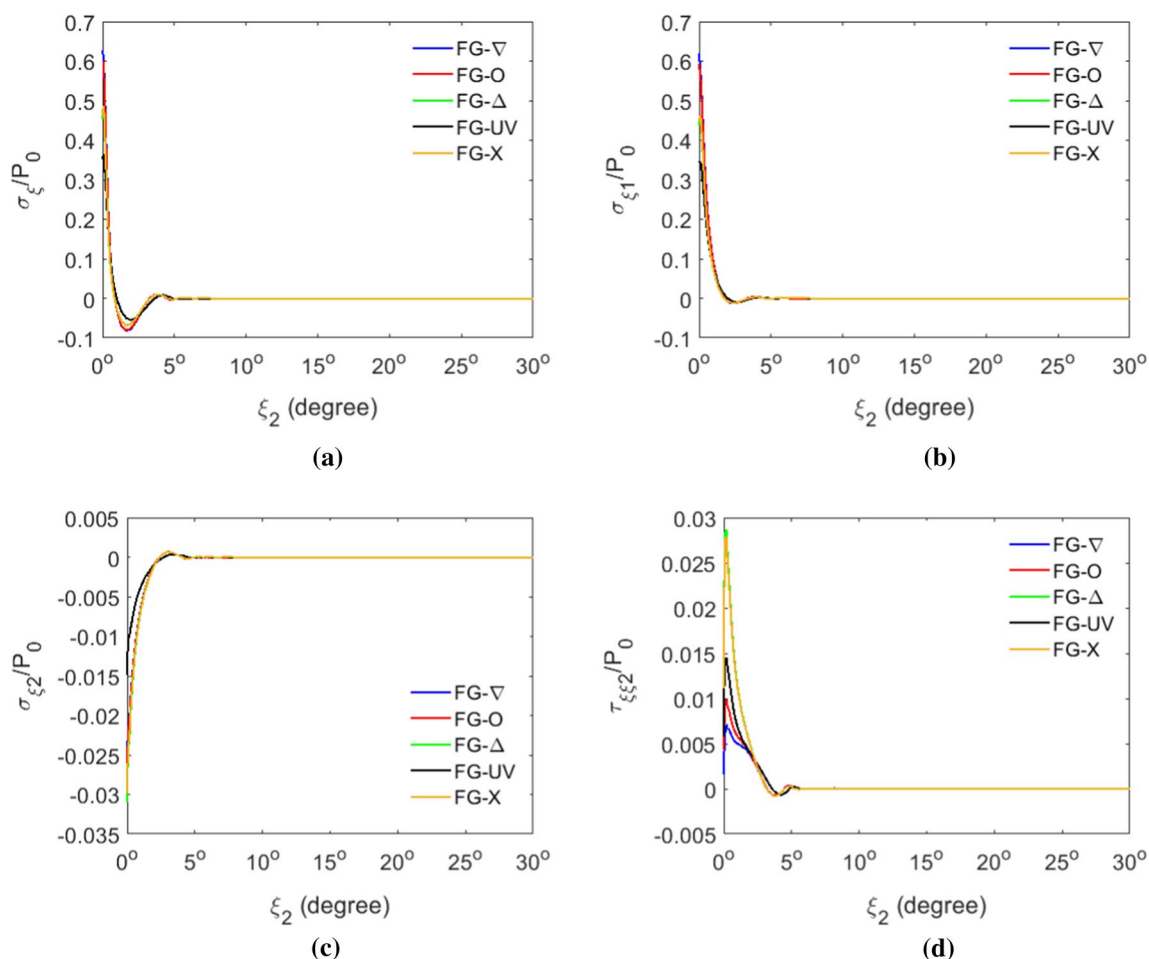


Fig. 7 The variation of the stress components in the top piezoelectric layer in terms of ξ_2 on path 2, **a** σ_ξ , **b** σ_{ξ_1} , **c** σ_{ξ_2} , **d** $\tau_{\xi\xi_2}$, for $h/R = 0.1, h_1/h = 0.1, R = 5 \text{ mm}$ and $\chi_0 = 30^\circ$

nanotubes are located in the bottom layer of the core relative to when they are made uniform leads to an increase in the meridian stress in the core.

Figure 9 shows the maximum radial, circumferential, and shear stresses on path 5, as well as the maximum meridian stress on path 3 at the core at $t = t_{\max}/2$. According to Fig. 9a, it can be seen that the radial stress has the maximum and minimum value in the samples FG-O and FG-UV, respectively. According to Fig. 9b, it can be seen that the circumferential stress has the maximum and minimum value in the samples FG-Δ and FG-UV, respectively. According to Fig. 9c, it can be seen that the meridian stress has the maximum and minimum value in the samples FG-∇ and FG-UV, respectively. According to Fig. 9d, it can be seen that the shear stress has the maximum and minimum value in the samples FG-Δ and FG-∇, respectively.

Figure 10 shows the maximum radial, circumferential, and meridian stresses on path 4, as well as the maximum shear stress on path 6 at the top piezoelectric face sheet at $t = t_{\max}/2$. According to Fig. 10, it can be seen that the maximum stress components in the sample FG-O are generated compared to the other four models of FG-CNT core. In addition, it can be seen that the minimum stress components in the sample FG-UV are generated compared to the other four models of FG-CNT core. This means that the top face sheet experiences more stress distribution when the nanotubes are located in the center of the core. Whereas, the top face sheet experiences minimal stress distribution when the nanotubes are made uniform in the core.

Figure 11 shows the variation of the voltage changes caused by the impact of the spherical elastic ball in the top face sheet layer at the point with spherical coordinate $(R + (h - h_3)/2, 0, 0)$. According to the figure, it can be

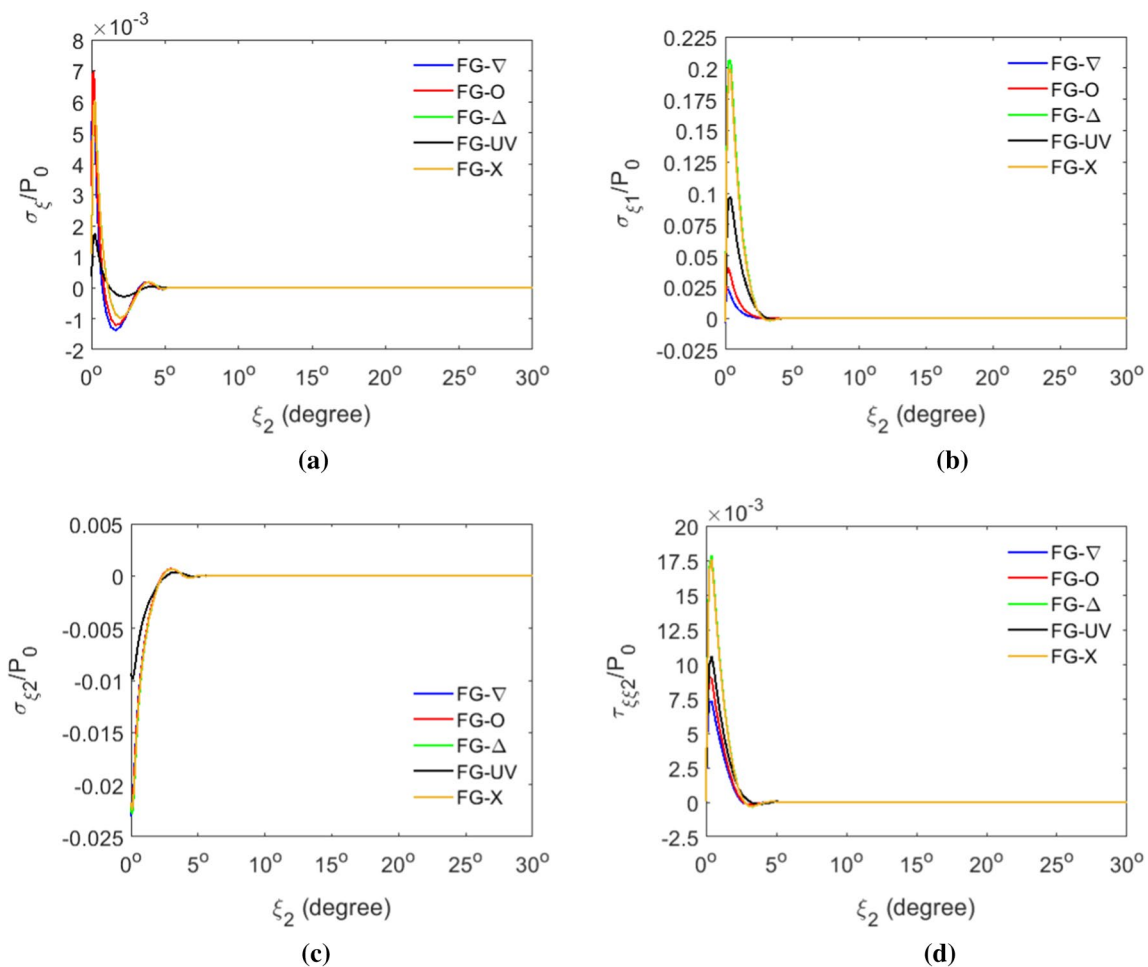


Fig. 8 The variation of the stress components in FG-CNT core in terms of ξ_2 on path 2, **a** σ_{ξ_1} , **b** σ_{ξ_2} , **c** σ_{ξ_3} , **d** $\tau_{\xi_1\xi_2}$, for $h/R = 0.1$, $h_1/h = 0.1$, $R = 5$ mm and $\chi_0 = 30^\circ$

observed that the impact phenomena lead to the production of the voltage in the piezoelectric layer in terms of time. Moreover, the maximum and minimum values of the voltage are generated in the sandwich sector with the samples FG-▽ and FG-X, respectively. Furthermore, it can be seen that for $t_{\max} \leq t$, the voltage acts as a damping function in terms of time and eventually becomes zero.

6 Conclusions

In the current study, a new theory solution was introduced in the field of layerwise theory along with higher-order shear deformation theory to calculate the stress distribution in the three-layer spherical sandwich shell subjected to the low-velocity impact. In order to solve the impact problem at the three-layer spherical sandwich shell, the sets of the nineteen nonlinear equations should be solved. The results showed that the sample of the FG-CNT core has more effect

on the stress distribution in the top face sheet. In addition, the results showed that the top face sheet experiences more stress distribution when the nanotubes are located in the center of the core. Moreover, the top face sheet experiences minimal stress distribution when the nanotubes are made uniform in the core.

According to the results, it can be observed that although the theoretical calculations of the present study are very complex and heavy, LT was able to efficiently solve the issue of the low-velocity impact in a three-layer spherical sector. Moreover, the advantages of the theory are categorized as follows:

- Solving the low-velocity impact issue of the three-layer sandwich sector with piezoelectric face sheets and FG-CNT core in less than 15 min with high accuracy.
- Ability to change the geometric dimensions as well as the mechanical properties of the layers and find relevant results, easily.

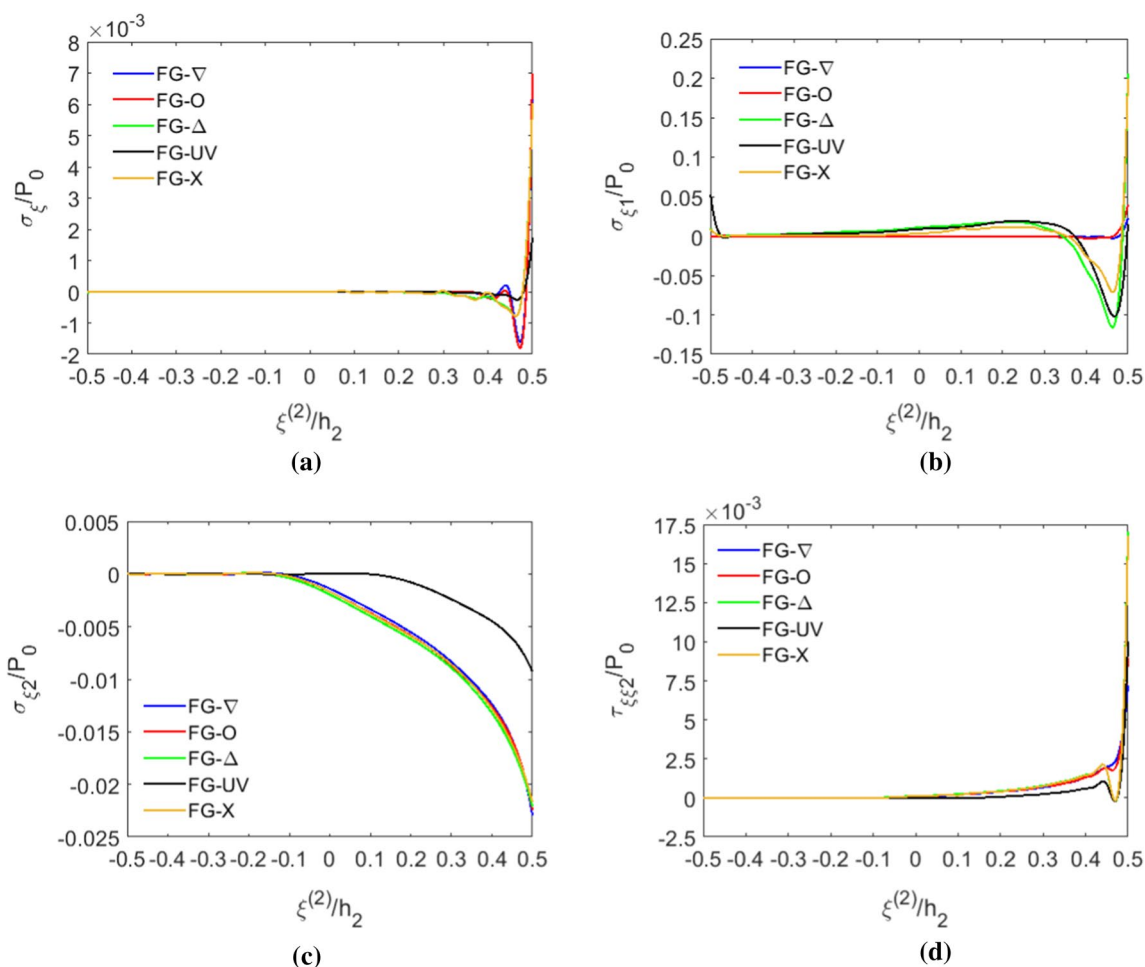


Fig. 9 The variation of the stress components in terms of $\xi^{(2)}/h_2$, **a** σ_{ξ} on path 5, **b** σ_{ξ_1} on path 5, **c** σ_{ξ_2} on path 3, **d** $\tau_{\xi\xi_2}$ on path 5, for $h/R = 0.1, h_1/h = 0.1, R = 5$ mm and $\chi_0 = 30^\circ$

Finally, the limitations of the current theoretical based on LT along with HSDT are:

- The other geometry of the structures
In complex geometries, due to the high volume of calculation, this method may not work well.
- When the issue of mechanical failure arises
Due to the mechanical failure, the geometry of the structure will certainly undergo a large deformed shape. The current study only can be used for small deformation and small strain.
- The classical non-adhesive elastic contact theory and Hunter’s relationship.

Due to the different nature of the high-velocity impact, this theory is not able to accurately estimate the contact pressure in terms of time and other parameters.

Appendix A

Expressions for the variation in modulus of elasticity, Poisson’s ratio, and density of the FG-CNT core along its thickness.

$$E_{11}(\xi) = \eta_1 V_{\text{CNT}}(\xi) E_{11}^{\text{CNT}} + V_m(\xi) E^m \tag{A1}$$

$$\frac{\eta_2}{E_{22}(\xi)} = \frac{V_{\text{CNT}}(\xi)}{E_{22}^{\text{CNT}}} + \frac{V_m(\xi)}{E^m} \tag{A2}$$

$$E_{33}(\xi) = E_{22}(\xi) \tag{A3}$$

$$\frac{\eta_3}{G_{12}(\xi)} = \frac{V_{\text{CNT}}(\xi)}{G_{12}^{\text{CNT}}} + \frac{V_m(\xi)}{G^m} \tag{A4}$$

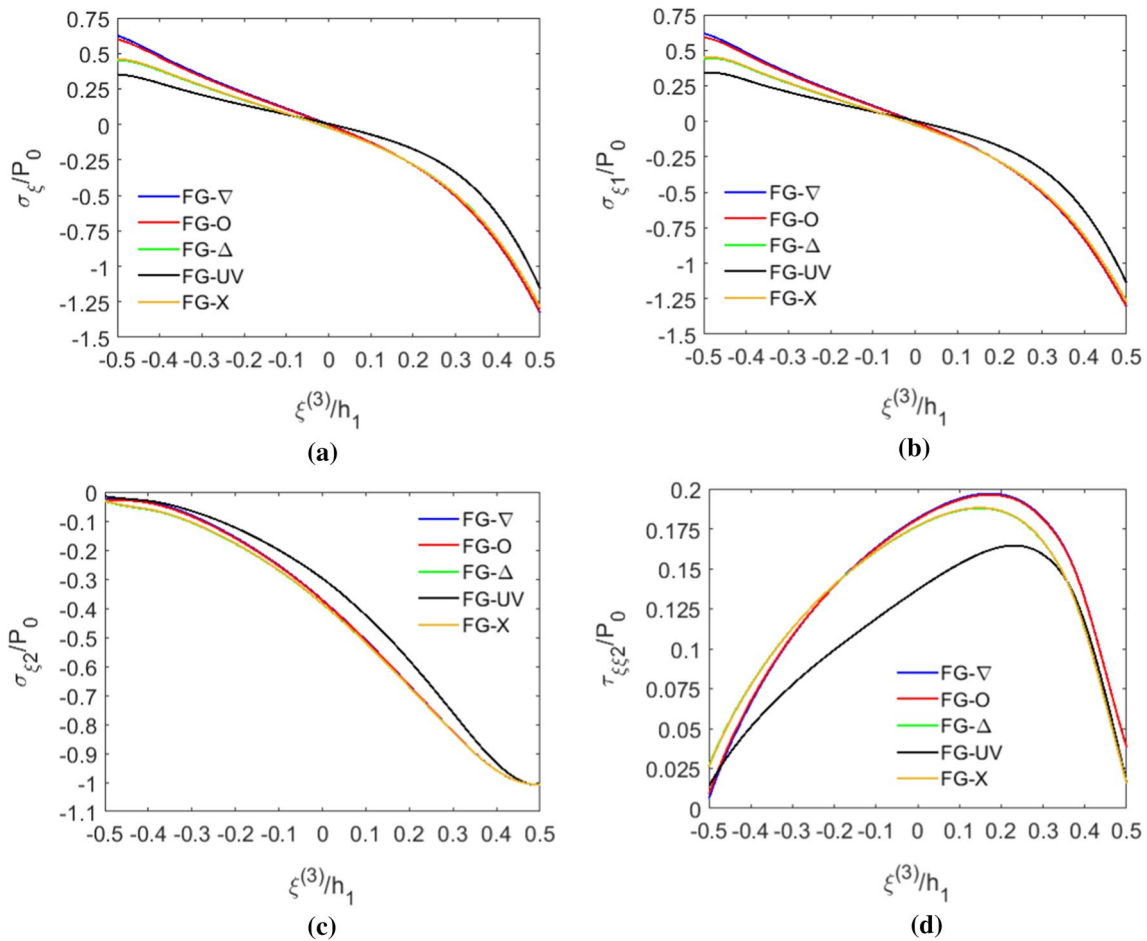


Fig. 10 The variation of the stress components in terms of $\xi^{(3)}/h_1$, **a** σ_x on path 4, **b** σ_{x_1} on path 4, **c** σ_{x_2} on path 4, **d** $\tau_{x_1x_2}$ on path 6, for $h/R = 0.1, h_1/h = 0.1, R = 5$ mm and $\chi_0 = 30^\circ$

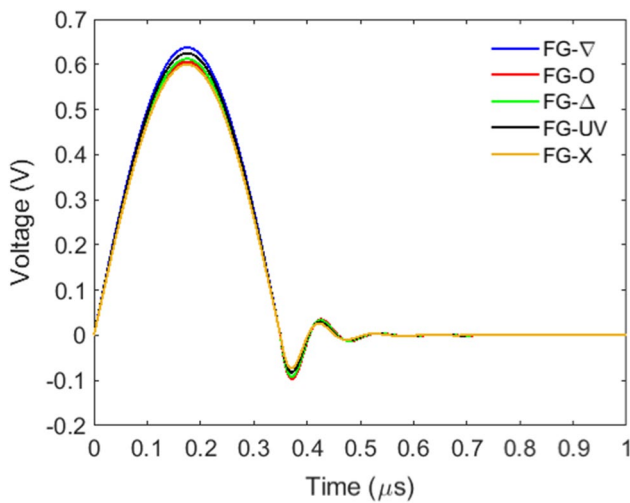


Fig. 11 The variation of the voltage changes caused by the impact of the spherical elastic ball in the top face sheet layer at the point with spherical coordinate $(R+(h-h_3)/2, 0, 0)$ for $h/R = 0.1, h_1/h = 0.1, R = 5$ mm and $\chi_0 = 30^\circ$

$$G_{13}(\xi) = G_{23}(\xi) = G_{12}(\xi) \tag{A5}$$

$$v_{12}(\xi) = V_{CNT}(\xi)v_{12}^{CNT} + V_m(\xi)v^m \tag{A6}$$

$$v_{21}(\xi) = \frac{v_{12}(\xi)}{E_{11}(\xi)}E_{22}(\xi) \tag{A7}$$

$$v_{13}(\xi) = v_{12}(\xi) \tag{A8}$$

$$v_{31}(\xi) = v_{21}(\xi) \tag{A9}$$

$$v_{32}(\xi) = v_{23}(\xi) = v_{21}(\xi) \tag{A10}$$

$$\rho(\xi) = V_{CNT}(\xi)\rho^{CNT} + V_m(\xi)\rho^m \tag{A11}$$

where

$$V_{CNT}(\xi) + V_m(\xi) = 1 \tag{A12}$$

$$V_{CNT}(\xi) = \Upsilon V_{CNT}^* \tag{A13}$$

$$Y = \begin{cases} 1 & \text{For FG-UV} \\ 1 + \frac{2\xi}{h_2} & \text{For FG-V} \\ 1 - \frac{2\xi}{h_2} & \text{For FG-}\Delta \\ 2\left(1 - \frac{2|\xi|}{h_2}\right) & \text{For FG-O} \\ 4\frac{|\xi|}{h_2} & \text{For FG-X} \end{cases} \tag{A14}$$

$$V_{\text{CNT}}^* = \frac{W_{\text{CNT}}}{W_{\text{CNT}} + \frac{\rho_{\text{CNT}}}{\rho^m}(1 - W_{\text{CNT}})} \tag{A15}$$

Appendix B

Expressions for the displacement components in the sandwich. In these equations, $\xi^{(k)}$ is measured from the k th layer mid-surface (see Fig. 1). Furthermore, it is assumed that $u_3^{(k)}$ ($k=1, 2$ and 3) is considered a function in terms of ξ_1, ξ_2 and $\xi^{(k)}$.

$$u_1^{(1)} = \begin{bmatrix} u_0 - \frac{h_2}{3}\psi_1^{(2)} - \frac{h_2^2}{8}\alpha_1^{(2)} - \frac{4}{3h_2^2}\beta_1^{(2)} + \frac{h_2^3}{24}\lambda_1^{(2)} - \frac{h_1}{3}\psi_1^{(1)} - \frac{h_1^2}{8}\alpha_1^{(1)} \\ -\frac{4}{3h_1^2}\beta_1^{(1)} + \frac{h_1^3}{24}\lambda_1^{(1)} + \left[\xi^{(1)} - \frac{4}{3h_1^2}\xi^{(1)^3}\right]\psi_1^{(1)} - \frac{1}{2}\xi^{(1)^2}\alpha_1^{(1)} \\ -\frac{4}{3h_1^2}\beta_1^{(1)} - \frac{1}{3}\xi^{(1)^3}\lambda_1^{(1)} \end{bmatrix} \tag{B1}$$

$$u_2^{(1)} = \begin{bmatrix} v_0 - \frac{h_2}{3}\psi_2^{(2)} - \frac{h_2^2}{8}\alpha_2^{(2)} - \frac{4}{3h_2^2}\beta_2^{(2)} + \frac{h_2^3}{24}\lambda_2^{(2)} - \frac{h_1}{3}\psi_2^{(1)} - \frac{h_1^2}{8}\alpha_2^{(1)} \\ -\frac{4}{3h_1^2}\beta_2^{(1)} + \frac{h_1^3}{24}\lambda_2^{(1)} + \left[\xi^{(1)} - \frac{4}{3h_1^2}\xi^{(1)^3}\right]\psi_2^{(1)} - \frac{1}{2}\xi^{(1)^2}\alpha_2^{(1)} \\ -\frac{4}{3h_1^2}\beta_2^{(1)} - \frac{1}{3}\xi^{(1)^3}\lambda_2^{(1)} \end{bmatrix} \tag{B2}$$

$$u_3^{(1)} = w_0 - \frac{h_2}{2}\psi_3^{(2)} + \frac{h_2^2}{4}\alpha_3^{(2)} - \frac{h_1}{2}\psi_3^{(1)} + \frac{h_1^2}{4}\alpha_3^{(1)} + \xi^{(1)}\psi_3^{(1)} + \xi^{(1)^2}\alpha_3^{(1)} \tag{B3}$$

$$u_1^{(2)} = u_0 + \left[\xi^{(2)} - \frac{4}{3h_2^2}\xi^{(2)^3}\right]\psi_1^{(2)} - \frac{1}{2}\xi^{(2)^2}\alpha_1^{(2)} - \frac{4}{3h_2^2}\beta_1^{(2)} - \frac{1}{3}\xi^{(2)^3}\lambda_1^{(2)} \tag{B4}$$

$$u_2^{(2)} = v_0 + \left[\xi^{(2)} - \frac{4}{3h_2^2}\xi^{(2)^3}\right]\psi_2^{(2)} - \frac{1}{2}\xi^{(2)^2}\alpha_2^{(2)} - \frac{4}{3h_2^2}\beta_2^{(2)} - \frac{1}{3}\xi^{(2)^3}\lambda_2^{(2)} \tag{B5}$$

$$u_3^{(2)} = w_0 + \xi^{(2)}\psi_3^{(2)} + \xi^{(2)^2}\alpha_3^{(2)} \tag{B6}$$

$$u_1^{(3)} = \begin{bmatrix} u_0 + \frac{h_2}{3}\psi_1^{(2)} - \frac{h_2^2}{8}\alpha_1^{(2)} - \frac{4}{3h_2^2}\beta_1^{(2)} - \frac{h_2^3}{24}\lambda_1^{(2)} + \frac{h_3}{3}\psi_1^{(3)} - \frac{h_3^2}{8}\alpha_1^{(3)} \\ -\frac{4}{3h_3^2}\beta_1^{(3)} - \frac{h_3^3}{24}\lambda_1^{(3)} + \left[\xi^{(3)} - \frac{4}{3h_3^2}\xi^{(3)^3}\right]\psi_1^{(3)} - \frac{1}{2}\xi^{(3)^2}\alpha_1^{(3)} \\ -\frac{4}{3h_3^2}\beta_1^{(3)} - \frac{1}{3}\xi^{(3)^3}\lambda_1^{(3)} \end{bmatrix} \tag{B7}$$

$$u_2^{(3)} = \begin{bmatrix} v_0 + \frac{h_2}{3}\psi_2^{(2)} - \frac{h_2^2}{8}\alpha_2^{(2)} - \frac{4}{3h_2^2}\beta_2^{(2)} - \frac{h_2^3}{24}\lambda_2^{(2)} + \frac{h_3}{3}\psi_2^{(3)} - \frac{h_3^2}{8}\alpha_2^{(3)} \\ -\frac{4}{3h_3^2}\beta_2^{(3)} - \frac{h_3^3}{24}\lambda_2^{(3)} + \left[\xi^{(3)} - \frac{4}{3h_3^2}\xi^{(3)^3}\right]\psi_2^{(3)} - \frac{1}{2}\xi^{(3)^2}\alpha_2^{(3)} \\ -\frac{4}{3h_3^2}\beta_2^{(3)} - \frac{1}{3}\xi^{(3)^3}\lambda_2^{(3)} \end{bmatrix} \tag{B8}$$

$$u_3^{(3)} = w_0 + \frac{h_2}{2}\psi_3^{(2)} + \frac{h_2^2}{4}\alpha_3^{(2)} + \frac{h_3}{2}\psi_3^{(3)} + \frac{h_3^2}{4}\alpha_3^{(3)} + \xi^{(3)}\psi_3^{(3)} + \xi^{(3)^2}\alpha_3^{(3)} \tag{B9}$$

Appendix C

Expressions for the displacement components and curvatures ($u_0, v_0, w_0, \psi_i^{(k)}, \alpha_i^{(k)}, \beta_j^{(k)}$ and $\lambda_j^{(k)}$ ($i=1, 2, 3; j=1, 2$ and $k=1, 2, 3$)) can be written as Eqs. (C1)–(C13) based on a simply supported boundary conditions for the spherical sandwich shell. In these equations, $u_{mn}, v_{mn}, w_{mn}, \psi_{i_{mn}}^{(k)}$ and $\alpha_{3_{mn}}^{(k)}$ ($i=1, 2, 3; k=1, 2, 3$), are the coefficients yet to be determined. Furthermore, m and n are ranging from 1 to infinity, to achieve a solution for each parameter given above, only 50,000 terms for both were used for a complete convergence.

$$u_0 = \sum_{m=1}^{\infty} \sum_{n=1}^{\infty} u_{mn} \cos(\omega\xi_1) \sin(\mu\xi_2) \tag{C1}$$

$$v_0 = \sum_{m=1}^{\infty} \sum_{n=1}^{\infty} v_{mn} \sin(\omega\xi_1) \cos(\mu\xi_2) \tag{C2}$$

$$w_0 = \sum_{m=1}^{\infty} \sum_{n=1}^{\infty} w_{mn} \sin(\omega\xi_1) \sin(\mu\xi_2) \tag{C3}$$

$$\psi_1^{(k)} = \sum_{m=1}^{\infty} \sum_{n=1}^{\infty} \psi_{1_{mn}}^{(k)} \cos(\omega\xi_1) \sin(\mu\xi_2) \tag{C4}$$

$$\psi_2^{(k)} = \sum_{m=1}^{\infty} \sum_{n=1}^{\infty} \psi_{2_{mn}}^{(k)} \sin(\omega\xi_1) \cos(\mu\xi_2) \tag{C5}$$

$$\psi_3^{(k)} = \sum_{m=1}^{\infty} \sum_{n=1}^{\infty} \psi_{3_{mn}}^{(k)} \sin(\omega\xi_1) \sin(\mu\xi_2) \tag{C6}$$

$$\alpha_1^{(k)} = \frac{\partial \psi_3^{(k)}}{\partial \xi_1} = \sum_{m=1}^{\infty} \sum_{n=1}^{\infty} \psi_{3_{mn}}^{(k)} \omega \cos(\omega\xi_1) \sin(\mu\xi_2) \tag{C7}$$

$$\alpha_2^{(k)} = \frac{\partial \psi_3^{(k)}}{\partial \xi_2} = \sum_{m=1}^{\infty} \sum_{n=1}^{\infty} \psi_{3_{mn}}^{(k)} \mu \sin(\omega\xi_1) \cos(\mu\xi_2) \tag{C8}$$

$$\alpha_3^{(k)} = \sum_{m=1}^{\infty} \sum_{n=1}^{\infty} \alpha_{3_{mn}}^{(k)} \sin(\omega \xi_1) \sin(\mu \xi_2) \tag{C9}$$

$$\beta_1^{(k)} = \frac{\partial w_0}{\partial \xi_1} = \sum_{m=1}^{\infty} \sum_{n=1}^{\infty} w_{mn} \omega \cos(\omega \xi_1) \sin(\mu \xi_2) \tag{C10}$$

$$\beta_2^{(k)} = \frac{\partial w_0}{\partial \xi_2} = \sum_{m=1}^{\infty} \sum_{n=1}^{\infty} w_{mn} \mu \sin(\omega \xi_1) \cos(\mu \xi_2) \tag{C11}$$

$$\lambda_1^{(k)} = \frac{\partial \alpha_3^{(k)}}{\partial \xi_1} = \sum_{m=1}^{\infty} \sum_{n=1}^{\infty} \alpha_{3_{mn}}^{(k)} \omega \cos(\omega \xi_1) \sin(\mu \xi_2) \tag{C12}$$

$$\lambda_2^{(k)} = \frac{\partial \alpha_3^{(k)}}{\partial \xi_2} = \sum_{m=1}^{\infty} \sum_{n=1}^{\infty} \alpha_{3_{mn}}^{(k)} \mu \sin(\omega \xi_1) \cos(\mu \xi_2) \tag{C13}$$

$$\begin{bmatrix} \sigma_{11}^{P(k)} \\ \sigma_{22}^{P(k)} \\ \sigma_{33}^{P(k)} \\ \tau_{13}^{P(k)} \\ \tau_{23}^{P(k)} \\ \tau_{12}^{P(k)} \end{bmatrix} = \begin{bmatrix} C_{11}^{(k)} & C_{12}^{(k)} & C_{13}^{(k)} & 0 & 0 & 0 \\ C_{12}^{(k)} & C_{22}^{(k)} & C_{23}^{(k)} & 0 & 0 & 0 \\ C_{13}^{(k)} & C_{23}^{(k)} & C_{33}^{(k)} & 0 & 0 & 0 \\ 0 & 0 & 0 & C_{44}^{(k)} & 0 & 0 \\ 0 & 0 & 0 & 0 & C_{55}^{(k)} & 0 \\ 0 & 0 & 0 & 0 & 0 & C_{66}^{(k)} \end{bmatrix} \begin{bmatrix} \epsilon_1^{(k)} \\ \epsilon_2^{(k)} \\ \epsilon_3^{(k)} \\ \gamma_{13}^{(k)} \\ \gamma_{23}^{(k)} \\ \gamma_{12}^{(k)} \end{bmatrix} - \begin{bmatrix} 0 & 0 & e_1 \\ 0 & 0 & e_2 \\ 0 & 0 & e_3 \\ 0 & e_4 & 0 \\ e_5 & 0 & 0 \\ 0 & 0 & 0 \end{bmatrix} \begin{bmatrix} E_1^{(k)} \\ E_2^{(k)} \\ E_3^{(k)} \end{bmatrix} \tag{D2}$$

for $k = 1, 3$.

Appendix D

Expressions for the stress–strain relation in the FG-CNT core and piezoelectric face sheets can be written as Eqs. (D1) and (D2), respectively. Moreover, the electric displacement relations for piezoelectric face sheets can be written as Eq. (D3).

$$\bar{D}^{(k)} = \begin{bmatrix} D_1^{(k)} \\ D_2^{(k)} \\ D_3^{(k)} \end{bmatrix} = \begin{bmatrix} 0 & 0 & 0 & 0 & e_5 & 0 \\ 0 & 0 & 0 & e_4 & 0 & 0 \\ e_1 & e_2 & e_3 & 0 & 0 & 0 \end{bmatrix} \begin{bmatrix} \epsilon_1^{(k)} \\ \epsilon_2^{(k)} \\ \epsilon_3^{(k)} \\ \gamma_{23}^{(k)} \\ \gamma_{13}^{(k)} \\ \gamma_{12}^{(k)} \end{bmatrix} \tag{D3}$$

$$+ \begin{bmatrix} \mu_1 & 0 & 0 \\ 0 & \mu_2 & 0 \\ 0 & 0 & \mu_3 \end{bmatrix} \begin{bmatrix} E_1^{(k)} \\ E_2^{(k)} \\ E_3^{(k)} \end{bmatrix} \text{ for } k = 1, 3.$$

$$\begin{bmatrix} \sigma_{11}^{(2)} \\ \sigma_{22}^{(2)} \\ \sigma_{33}^{(2)} \\ \tau_{13}^{(2)} \\ \tau_{23}^{(2)} \\ \tau_{12}^{(2)} \end{bmatrix} = \begin{bmatrix} Q_{11}^{(2)} & Q_{12}^{(2)} & Q_{13}^{(2)} & 0 & 0 & 0 \\ Q_{12}^{(2)} & Q_{22}^{(2)} & Q_{23}^{(2)} & 0 & 0 & 0 \\ Q_{13}^{(2)} & Q_{23}^{(2)} & Q_{33}^{(2)} & 0 & 0 & 0 \\ 0 & 0 & 0 & Q_{44}^{(2)} & 0 & 0 \\ 0 & 0 & 0 & 0 & Q_{55}^{(2)} & 0 \\ 0 & 0 & 0 & 0 & 0 & Q_{66}^{(2)} \end{bmatrix} \begin{bmatrix} \epsilon_1^{(2)} \\ \epsilon_2^{(2)} \\ \epsilon_3^{(2)} \\ \gamma_{13}^{(2)} \\ \gamma_{23}^{(2)} \\ \gamma_{12}^{(2)} \end{bmatrix} \tag{D1}$$

where

$$\begin{cases} Q_{11}^{(2)} = \frac{E_{11}^{(2)}}{\Delta^{(2)}} (1 - \nu_{23}^{(2)} \nu_{32}^{(2)}); Q_{22}^{(2)} = \frac{E_{22}^{(2)}}{\Delta^{(2)}} (1 - \nu_{13}^{(2)} \nu_{31}^{(2)}); \\ Q_{33}^{(2)} = \frac{E_{33}^{(2)}}{\Delta^{(2)}} (1 - \nu_{12}^{(2)} \nu_{21}^{(2)}); Q_{12}^{(2)} = \frac{E_{11}^{(2)}}{\Delta^{(2)}} (\nu_{21}^{(2)} + \nu_{31}^{(2)} \nu_{23}^{(2)}); \\ Q_{13}^{(2)} = \frac{E_{11}^{(2)}}{\Delta^{(2)}} (\nu_{31}^{(2)} + \nu_{21}^{(2)} \nu_{32}^{(2)}); Q_{23}^{(2)} = \frac{E_{22}^{(2)}}{\Delta^{(2)}} (\nu_{32}^{(2)} + \nu_{12}^{(2)} \nu_{31}^{(2)}); \\ Q_{44}^{(2)} = G_{23}^{(2)}; Q_{55}^{(2)} = G_{13}^{(2)}; Q_{66}^{(2)} = G_{12}^{(2)}; \\ \Delta^{(2)} = 1 - \nu_{12}^{(2)} \nu_{21}^{(2)} - \nu_{23}^{(2)} \nu_{32}^{(2)} - \nu_{13}^{(2)} \nu_{31}^{(2)} - 2\nu_{12}^{(2)} \nu_{32}^{(2)} \nu_{13}^{(2)}. \end{cases} \tag{D4}$$

$$E_1^{(k)} = -\frac{1}{r^{(k)} \sin \xi_2} \frac{\partial \Phi^{(k)}}{\partial \xi_1}; E_2^{(k)} = -\frac{1}{r^{(k)}} \frac{\partial \Phi^{(k)}}{\partial \xi_2}; E_3^{(k)} = -\frac{\partial \Phi^{(k)}}{\partial \xi}; \text{ for } k = 1, 3. \tag{D5}$$

Appendix E

Expressions for the virtual kinetic energy (E1) and the virtual strain energy (E3).

where in Eq. (E1), $I_q^{(k)}$ ($k = 1, 2, 3$ and $q = 0, 1, 2, 3, 4, 5, 6$) is defined as Eq. (E2).

$$I_q^{(k)} = \int_{-\frac{h_k}{2}}^{\frac{h_k}{2}} \rho^{(k)} \xi^{(k)q} \left(1 + \frac{\xi^{(k)}}{r^{(k)}} \right) d\xi^{(k)}; \quad \text{where } k = 1, 2, 3 \text{ and } q = 0, 1, 2, 3, 4, 5, 6. \tag{E2}$$

$$\delta U = \int_{\Omega} \left\{ \begin{aligned} & \left(\sum_{k=1}^3 \left(\frac{1}{r^{(k)}} \left[\frac{1}{\sin \xi_2} \frac{\partial N_{11}^{(k)}}{\partial \xi_1} - N_{13}^{(k)} + \frac{\partial N_{12}^{(k)}}{\partial \xi_2} - N_{12}^{(k)} \cot \xi_2 \right] \right) \right) \delta u_0 \\ & + \left(-\frac{h_1}{3r^{(1)}} \left[\frac{1}{\sin \xi_2} \frac{\partial N_{11}^{(1)}}{\partial \xi_1} + \frac{\partial N_{12}^{(1)}}{\partial \xi_2} \right] - \frac{1}{r^{(1)}} \left[\frac{1}{\sin \xi_2} \frac{\partial M_{11}^{(1)}}{\partial \xi_1} + \frac{\partial M_{12}^{(1)}}{\partial \xi_2} - \frac{4}{3h_1^2} \left(\frac{1}{\sin \xi_2} \frac{\partial q_{11}^{(1)}}{\partial \xi_1} + \frac{\partial q_{12}^{(1)}}{\partial \xi_2} \right) \right] \right. \\ & \left. + \left[\left(1 + \frac{h_1}{3r^{(1)}} \right) N_{13}^{(1)} + \frac{h_1}{3r^{(1)}} N_{12}^{(1)} \cot \xi_2 - \frac{4}{h_1^2} P_{13}^{(1)} \right] + \frac{1}{r^{(1)}} \left[M_{13}^{(1)} + M_{12}^{(1)} \cot \xi_2 - \frac{4}{3h_1^2} \left(q_{13}^{(1)} + q_{12}^{(1)} \cot \xi_2 \right) \right] \right) \delta \psi_1^{(1)} \\ & + \left(\frac{h_2}{3 \sin \xi_2} \left[\frac{1}{r^{(1)}} \frac{\partial N_{11}^{(1)}}{\partial \xi_1} - \frac{1}{r^{(3)}} \frac{\partial N_{11}^{(3)}}{\partial \xi_1} \right] + \frac{h_2}{3} \left[\frac{1}{r^{(1)}} \frac{\partial N_{12}^{(1)}}{\partial \xi_2} - \frac{1}{r^{(3)}} \frac{\partial N_{12}^{(3)}}{\partial \xi_2} \right] - \frac{1}{r^{(2)}} \left[\frac{1}{\sin \xi_2} \frac{\partial M_{11}^{(2)}}{\partial \xi_1} + \frac{\partial M_{12}^{(2)}}{\partial \xi_2} - \frac{4}{3h_2^2} \left(\frac{1}{\sin \xi_2} \frac{\partial q_{11}^{(2)}}{\partial \xi_1} + \frac{\partial q_{12}^{(2)}}{\partial \xi_2} \right) \right] \right. \\ & \left. + \left[N_{13}^{(2)} - \frac{4}{h_2^2} P_{13}^{(2)} \right] + \frac{1}{r^{(2)}} \left[M_{13}^{(2)} + M_{12}^{(2)} \cot \xi_2 - \frac{4}{3h_2^2} \left(q_{13}^{(2)} + q_{12}^{(2)} \cot \xi_2 \right) \right] + \frac{h_2}{3} \left[-\frac{N_{13}^{(1)}}{r^{(1)}} - \frac{N_{12}^{(1)}}{r^{(1)}} \cot \xi_2 + \frac{N_{13}^{(3)}}{r^{(3)}} + \frac{N_{12}^{(3)}}{r^{(3)}} \cot \xi_2 \right] \right) \delta \psi_1^{(2)} \\ & + \left(\frac{h_3}{3r^{(3)}} \left[\frac{1}{\sin \xi_2} \frac{\partial N_{11}^{(3)}}{\partial \xi_1} + \frac{\partial N_{12}^{(3)}}{\partial \xi_2} \right] - \frac{1}{r^{(3)}} \left[\frac{1}{\sin \xi_2} \frac{\partial M_{11}^{(3)}}{\partial \xi_1} + \frac{\partial M_{12}^{(3)}}{\partial \xi_2} - \frac{4}{3h_3^2} \left(\frac{1}{\sin \xi_2} \frac{\partial q_{11}^{(3)}}{\partial \xi_1} + \frac{\partial q_{12}^{(3)}}{\partial \xi_2} \right) \right] \right. \\ & \left. + \left[\left(1 - \frac{h_3}{3r^{(3)}} \right) N_{13}^{(3)} - \frac{h_3}{3r^{(3)}} N_{12}^{(3)} \cot \xi_2 - \frac{4}{h_3^2} P_{13}^{(3)} \right] + \frac{1}{r^{(3)}} \left[M_{13}^{(3)} + M_{12}^{(3)} \cot \xi_2 - \frac{4}{3h_3^2} \left(q_{13}^{(3)} + q_{12}^{(3)} \cot \xi_2 \right) \right] \right) \delta \psi_1^{(3)} \\ & + \left(\sum_{k=1}^3 \left(\frac{1}{r^{(k)}} \left[N_{11}^{(k)} \cot \xi_2 + \frac{\partial N_{22}^{(k)}}{\partial \xi_2} + \frac{1}{\sin \xi_2} \frac{\partial N_{12}^{(k)}}{\partial \xi_1} - N_{23}^{(k)} \right] \right) \right) \delta v_0 \\ & + \left(-\frac{h_1}{3r^{(1)}} \left[\frac{1}{\sin \xi_2} \frac{\partial N_{12}^{(1)}}{\partial \xi_1} + \frac{\partial N_{22}^{(1)}}{\partial \xi_2} \right] - \frac{1}{r^{(1)}} \left[\frac{1}{\sin \xi_2} \frac{\partial M_{12}^{(1)}}{\partial \xi_1} + \frac{\partial M_{22}^{(1)}}{\partial \xi_2} - \frac{4}{3h_1^2} \left(\frac{1}{\sin \xi_2} \frac{\partial q_{12}^{(1)}}{\partial \xi_1} + \frac{\partial q_{22}^{(1)}}{\partial \xi_2} \right) \right] \right. \\ & \left. - \frac{h_1}{3r^{(1)}} N_{11}^{(1)} \cot \xi_2 + \left(1 + \frac{h_1}{3r^{(1)}} \right) N_{23}^{(1)} - \frac{4}{h_1^2} P_{23}^{(1)} - \frac{1}{r^{(1)}} \left[M_{11}^{(1)} \cot \xi_2 - M_{23}^{(1)} - \frac{4}{3h_1^2} \left(q_{11}^{(1)} \cot \xi_2 - q_{23}^{(1)} \right) \right] \right) \delta \psi_2^{(1)} \\ & + \left(\frac{h_2}{3 \sin \xi_2} \left[\frac{1}{r^{(1)}} \frac{\partial N_{12}^{(1)}}{\partial \xi_1} - \frac{1}{r^{(3)}} \frac{\partial N_{12}^{(3)}}{\partial \xi_1} \right] + \frac{h_2}{3} \left[\frac{1}{r^{(1)}} \frac{\partial N_{22}^{(1)}}{\partial \xi_2} - \frac{1}{r^{(3)}} \frac{\partial N_{22}^{(3)}}{\partial \xi_2} \right] - \frac{1}{r^{(2)}} \left[\frac{1}{\sin \xi_2} \frac{\partial M_{12}^{(2)}}{\partial \xi_1} + \frac{\partial M_{22}^{(2)}}{\partial \xi_2} - \frac{4}{3h_2^2} \left(\frac{1}{\sin \xi_2} \frac{\partial q_{12}^{(2)}}{\partial \xi_1} + \frac{\partial q_{22}^{(2)}}{\partial \xi_2} \right) \right] \right. \\ & \left. - \frac{1}{r^{(2)}} \left[M_{11}^{(2)} \cot \xi_2 + M_{23}^{(2)} - \frac{4}{3h_2^2} \left(q_{11}^{(2)} \cot \xi_2 + q_{23}^{(2)} \right) \right] + \left[N_{23}^{(2)} - \frac{4}{h_2^2} P_{23}^{(2)} \right] + \frac{h_2}{3} \left[\frac{N_{11}^{(1)}}{r^{(1)}} \cot \xi_2 - \frac{N_{13}^{(1)}}{r^{(1)}} - \frac{N_{11}^{(3)}}{r^{(3)}} \cot \xi_2 + \frac{N_{23}^{(3)}}{r^{(3)}} \right] \right) \delta \psi_2^{(2)} \\ & + \left(\frac{h_3}{3r^{(3)}} \left[\frac{1}{\sin \xi_2} \frac{\partial N_{12}^{(3)}}{\partial \xi_1} + \frac{\partial N_{22}^{(3)}}{\partial \xi_2} \right] - \frac{1}{r^{(3)}} \left[\frac{1}{\sin \xi_2} \frac{\partial M_{12}^{(3)}}{\partial \xi_1} + \frac{\partial M_{22}^{(3)}}{\partial \xi_2} - \frac{4}{3h_3^2} \left(\frac{1}{\sin \xi_2} \frac{\partial q_{12}^{(3)}}{\partial \xi_1} + \frac{\partial q_{22}^{(3)}}{\partial \xi_2} \right) \right] \right. \\ & \left. + \frac{h_3}{3r^{(3)}} N_{11}^{(3)} \cot \xi_2 + \left(1 - \frac{h_3}{3r^{(3)}} \right) N_{23}^{(3)} - \frac{4}{h_3^2} P_{23}^{(3)} - \frac{1}{r^{(3)}} \left[M_{11}^{(3)} \cot \xi_2 - M_{23}^{(3)} - \frac{4}{3h_3^2} \left(q_{11}^{(3)} \cot \xi_2 - q_{23}^{(3)} \right) \right] \right) \delta \psi_2^{(3)} \\ & + \left(\sum_{k=1}^3 \left(\frac{1}{r^{(k)}} \left[N_{11}^{(k)} + N_{22}^{(k)} + \frac{\partial N_{23}^{(k)}}{\partial \xi_2} + \frac{1}{\sin \xi_2} \frac{\partial N_{13}^{(k)}}{\partial \xi_1} \right] \right) \right) \delta w_0 \\ & + \left(-\frac{h_1}{2r^{(1)}} \left[\frac{1}{\sin \xi_2} \frac{\partial N_{13}^{(1)}}{\partial \xi_1} + \frac{\partial N_{23}^{(1)}}{\partial \xi_2} + N_{11}^{(1)} + N_{22}^{(1)} \right] - \frac{1}{r^{(1)}} \left[\frac{1}{\sin \xi_2} \frac{\partial M_{13}^{(1)}}{\partial \xi_1} + \frac{\partial M_{23}^{(1)}}{\partial \xi_2} + M_{11}^{(1)} + M_{22}^{(1)} \right] + N_{33}^{(1)} \right) \delta \psi_3^{(1)} \\ & + \left(\frac{h_2}{2} \left[\frac{1}{r^{(1)}} \left(\frac{1}{\sin \xi_2} \frac{\partial N_{13}^{(1)}}{\partial \xi_1} + \frac{\partial N_{23}^{(1)}}{\partial \xi_2} \right) - \frac{1}{r^{(3)}} \left(\frac{1}{\sin \xi_2} \frac{\partial N_{13}^{(3)}}{\partial \xi_1} + \frac{\partial N_{23}^{(3)}}{\partial \xi_2} \right) \right] - \frac{1}{r^{(2)}} \left[\frac{1}{\sin \xi_2} \frac{\partial M_{13}^{(2)}}{\partial \xi_1} + \frac{\partial M_{23}^{(2)}}{\partial \xi_2} \right] + \frac{h_2}{2} \left[\frac{N_{11}^{(1)}}{r^{(1)}} + \frac{N_{22}^{(1)}}{r^{(1)}} - \frac{N_{11}^{(3)}}{r^{(3)}} - \frac{N_{22}^{(3)}}{r^{(3)}} \right] \right. \\ & \left. - \frac{1}{r^{(2)}} \left[M_{11}^{(2)} + M_{22}^{(2)} \right] + N_{33}^{(2)} \right) \delta \psi_3^{(2)} \\ & + \left(\frac{h_3}{2r^{(3)}} \left[\frac{1}{\sin \xi_2} \frac{\partial N_{13}^{(3)}}{\partial \xi_1} + \frac{\partial N_{23}^{(3)}}{\partial \xi_2} + N_{11}^{(3)} + N_{22}^{(3)} \right] - \frac{1}{r^{(3)}} \left[\frac{1}{\sin \xi_2} \frac{\partial M_{13}^{(3)}}{\partial \xi_1} + \frac{\partial M_{23}^{(3)}}{\partial \xi_2} + M_{11}^{(3)} + M_{22}^{(3)} \right] + N_{33}^{(3)} \right) \delta \psi_3^{(3)} \\ & + \left(\frac{h_1^2}{4r^{(1)}} \left[\frac{1}{\sin \xi_2} \frac{\partial N_{13}^{(1)}}{\partial \xi_1} + \frac{\partial N_{23}^{(1)}}{\partial \xi_2} + N_{11}^{(1)} + N_{22}^{(1)} \right] + \frac{1}{r^{(1)}} \left[\frac{1}{\sin \xi_2} \frac{\partial P_{13}^{(1)}}{\partial \xi_1} + \frac{\partial P_{23}^{(1)}}{\partial \xi_2} + P_{11}^{(1)} + P_{22}^{(1)} \right] - 2M_{33}^{(1)} \right) \delta \alpha_3^{(1)} \\ & + \left(\frac{1}{r^{(2)}} \left[\frac{1}{\sin \xi_2} \frac{\partial P_{13}^{(2)}}{\partial \xi_1} + \frac{\partial P_{23}^{(2)}}{\partial \xi_2} + P_{11}^{(2)} + P_{22}^{(2)} \right] - \frac{h_2^2}{4} \left[\frac{1}{r^{(1)}} \left(\frac{1}{\sin \xi_2} \frac{\partial N_{13}^{(1)}}{\partial \xi_1} + \frac{\partial N_{23}^{(1)}}{\partial \xi_2} + N_{11}^{(1)} + N_{22}^{(1)} \right) + \right. \right. \\ & \left. \left. \frac{1}{r^{(3)}} \left(\frac{1}{\sin \xi_2} \frac{\partial N_{13}^{(3)}}{\partial \xi_1} + \frac{\partial N_{23}^{(3)}}{\partial \xi_2} + N_{11}^{(3)} + N_{22}^{(3)} \right) \right] - 2M_{33}^{(2)} \right) \delta \alpha_3^{(2)} \\ & + \left(\frac{h_3^2}{4r^{(3)}} \left[\frac{1}{\sin \xi_2} \frac{\partial N_{13}^{(3)}}{\partial \xi_1} + \frac{\partial N_{23}^{(3)}}{\partial \xi_2} + N_{11}^{(3)} + N_{22}^{(3)} \right] + \frac{1}{r^{(3)}} \left[\frac{1}{\sin \xi_2} \frac{\partial P_{13}^{(3)}}{\partial \xi_1} + \frac{\partial P_{23}^{(3)}}{\partial \xi_2} + P_{11}^{(3)} + P_{22}^{(3)} \right] - 2M_{33}^{(3)} \right) \delta \alpha_3^{(3)} \\ & + \left(\frac{1}{\sin \xi_2} \frac{\partial \Gamma_1^{(1)}}{\partial \xi_1} + \frac{\partial \Gamma_2^{(1)}}{\partial \xi_1} - \Gamma_3^{(1)} \right) \delta \varphi^{(1)} + \left(\frac{1}{\sin \xi_2} \frac{\partial \Gamma_1^{(3)}}{\partial \xi_1} + \frac{\partial \Gamma_2^{(3)}}{\partial \xi_1} - \Gamma_3^{(3)} \right) \delta \varphi^{(3)} + \dots \end{aligned} \right\} d\xi_1 d\xi_2 \tag{E3}$$

where in Eq. (E3), $N_{ij}^{(k)}$, $M_{ij}^{(k)}$, $P_{ij}^{(k)}$, $q_{ij}^{(k)}$ and $\Gamma^{(k')}$ ($k = 1, 2, 3$ and $k' = 1, 3$) are defined as Eqs. (E4)–(E7).

$$\begin{bmatrix} N_{11}^{(k)} \\ N_{22}^{(k)} \\ N_{12}^{(k)} \\ M_{11}^{(k)} \\ M_{22}^{(k)} \\ M_{12}^{(k)} \\ P_{12}^{(k)} \\ P_{12}^{(k)} \\ P_{12}^{(k)} \\ q_{12}^{(k)} \\ q_{12}^{(k)} \\ q_{12}^{(k)} \end{bmatrix} = \begin{bmatrix} [A]^{(k)} & [B]^{(k)} & [D]^{(k)} & [E]^{(k)} \\ [B]^{(k)} & [D]^{(k)} & [E]^{(k)} & [F]^{(k)} \\ [D]^{(k)} & [E]^{(k)} & [F]^{(k)} & [G]^{(k)} \\ [E]^{(k)} & [F]^{(k)} & [G]^{(k)} & [H]^{(k)} \end{bmatrix} \begin{bmatrix} \epsilon_{11}^{0(k)} \\ \epsilon_{22}^{0(k)} \\ \gamma_{12}^{0(k)} \\ \epsilon_{11}^{1(k)} \\ \epsilon_{22}^{1(k)} \\ \gamma_{12}^{1(k)} \\ \epsilon_{11}^{2(k)} \\ \epsilon_{22}^{2(k)} \\ \gamma_{12}^{2(k)} \\ \epsilon_{11}^{3(k)} \\ \epsilon_{22}^{3(k)} \\ \gamma_{12}^{3(k)} \end{bmatrix} \tag{E4}$$

$$\begin{bmatrix} N_{13}^{(k)} \\ N_{23}^{(k)} \\ M_{13}^{(k)} \\ M_{23}^{(k)} \\ P_{13}^{(k)} \\ P_{23}^{(k)} \end{bmatrix} = \begin{bmatrix} A_{55}^{(k)} & 0 & B_{55}^{(k)} & 0 & D_{55}^{(k)} & 0 \\ 0 & A_{44}^{(k)} & 0 & B_{44}^{(k)} & 0 & D_{44}^{(k)} \\ B_{55}^{(k)} & 0 & D_{55}^{(k)} & 0 & E_{55}^{(k)} & 0 \\ 0 & B_{44}^{(k)} & 0 & D_{44}^{(k)} & 0 & E_{44}^{(k)} \\ D_{55}^{(k)} & 0 & E_{55}^{(k)} & 0 & F_{55}^{(k)} & 0 \\ 0 & D_{44}^{(k)} & 0 & E_{44}^{(k)} & 0 & F_{44}^{(k)} \end{bmatrix} \begin{bmatrix} \gamma_{13}^{0(k)} \\ \gamma_{23}^{0(k)} \\ \gamma_{13}^{1(k)} \\ \gamma_{23}^{1(k)} \\ \gamma_{13}^{2(k)} \\ \gamma_{23}^{2(k)} \end{bmatrix} \tag{E5}$$

$$\begin{bmatrix} N_{33}^{(k)} \\ M_{33}^{(k)} \end{bmatrix} = \begin{bmatrix} A_{33}^{(k)} & B_{33}^{(k)} \\ B_{33}^{(k)} & D_{33}^{(k)} \end{bmatrix} \begin{bmatrix} \epsilon_{33}^{0(k)} \\ \epsilon_{33}^{1(k)} \end{bmatrix} \tag{E6}$$

$$\begin{bmatrix} \Gamma_1^{(k')} \\ \Gamma_2^{(k')} \\ \Gamma_3^{(k')} \end{bmatrix} = \int_{-\frac{h_{k'}}{2}}^{\frac{h_{k'}}{2}} \begin{bmatrix} D_1^{(k')} \Phi^{(k')} \\ D_2^{(k')} \Phi^{(k')} \\ D_3^{(k')} \Phi^{(k')} \end{bmatrix} d\xi^{(k')} \tag{E7}$$

where the elements of matrices A, B, D, E, F, G and H ($k = 1, 2, 3$) are given as;

$$\begin{aligned} & (A_{ij}^{(k)}, B_{ij}^{(k)}, D_{ij}^{(k)}, E_{ij}^{(k)}, F_{ij}^{(k)}, G_{ij}^{(k)}, H_{ij}^{(k)}) \\ & = \int_{-\frac{h_k}{2}}^{\frac{h_k}{2}} Q_{ij}^{(k)} (1, \xi^{(k)}, \xi^{(k)2}, \xi^{(k)3}, \xi^{(k)4}, \xi^{(k)5}, \xi^{(k)6}) d\xi^{(k)} \tag{E8} \end{aligned}$$

for $i, j = 1, 2, 6$.

$$\begin{aligned} & (A_{ii}^{(k)}, B_{ii}^{(k)}, D_{ii}^{(k)}, E_{ii}^{(k)}, F_{ii}^{(k)}) \\ & = \int_{-\frac{h_k}{2}}^{\frac{h_k}{2}} Q_{ii}^{(k)} (1, \xi^{(k)}, \xi^{(k)2}, \xi^{(k)3}, \xi^{(k)4}) d\xi^{(k)} \text{ for } i = 4, 5. \tag{E9} \end{aligned}$$

$$(A_{33}^{(k)}, B_{33}^{(k)}, D_{33}^{(k)}) = \int_{-\frac{h_k}{2}}^{\frac{h_k}{2}} Q_{33}^{(k)} (1, \xi^{(k)}, \xi^{(k)2}) d\xi^{(k)} \tag{E10}$$

Funding This research did not receive any specific grant from funding agencies in the public, commercial, or not-for-profit sectors.

References

1. Cestino E, Romeo G, Piana P, Danzi F (2016) Numerical/experimental evaluation of buckling behaviour and residual tensile strength of composite aerospace structures after low velocity impact. *Aerosp Sci Technol* 54:1–9. <https://doi.org/10.1016/j.ast.2016.04.001>
2. Bikakis GSE (2017) Simulation of the dynamic response of GLARE plates subjected to low velocity impact using a linearized spring–mass model. *Aerosp Sci Technol* 64:24–30. <https://doi.org/10.1016/j.ast.2017.01.013>
3. Yellur MR, Seidlitz H, Kuke F, Wartig K, Tsombanis N (2019) A low velocity impact study on press formed thermoplastic

- honeycomb sandwich panels. *Compos Struct* 225:111061. <https://doi.org/10.1016/j.compstruct.2019.111061>
4. Saleh MN, Dessouky HME, Saeedifar M, Freitas STD, Scaife RJ, Zarouchas D (2019) Compression after multiple low velocity impacts of NCF, 2D and 3D woven composites. *Compos A* 125:105576. <https://doi.org/10.1016/j.compositesa.2019.105576>
 5. Kareem MG, Majeed WI (2019) Transient dynamic analysis of laminated shallow spherical shell under low-velocity impact. *J Market Res* 8:5283–5300. <https://doi.org/10.1016/j.jmrt.2019.08.050>
 6. Gao Q, Liao WH, Wang L (2020) On the low-velocity impact responses of auxetic double arrowed honeycomb. *Aerosp Sci Technol* 98:105698. <https://doi.org/10.1016/j.ast.2020.105698>
 7. Mohammed R, Zhang F, Sun B, Gu B (2013) Finite element analyses of low-velocity impact damage of foam sandwiched composites with different ply angles face sheets. *Mater Des* 47:189–199. <https://doi.org/10.1016/j.matdes.2012.12.016>
 8. Mao YQ, Fu YM, Chen CP, Li YL (2011) Nonlinear dynamic response for functionally graded shallow spherical shell under low velocity impact in thermal environment. *Appl Math Model* 35:2887–2900. <https://doi.org/10.1016/j.apm.2010.12.012>
 9. Lei ZX, Tong LH (2019) Analytical solution of low-velocity impact of graphene-reinforced composite functionally graded cylindrical shells. *J Braz Soc Mech Sci Eng* 41:486. <https://doi.org/10.1007/s40430-019-1983-5>
 10. Khodadadi A, Liaghat G, Ghafarokhi DS, Chizari M, Wang B (2020) Numerical and experimental investigation of impact on bilayer aluminum-rubber composite plate. *Thin Walled Struct* 149:106673. <https://doi.org/10.1016/j.tws.2020.106673>
 11. Sy BL, Fawaz Z, Bougherara H (2019) Numerical simulation correlating the low velocity impact behaviour of flax/epoxy laminates. *Compos A* 126:105582. <https://doi.org/10.1016/j.compositesa.2019.105582>
 12. Erklig A, Dogan NF (2020) Nanographene inclusion effect on the mechanical and low velocity impact response of glass/basalt reinforced epoxy hybrid nanocomposites. *J Braz Soc Mech Sci Eng* 42:83. <https://doi.org/10.1007/s40430-019-2168-y>
 13. Yao L, Wang C, He W, Lu S, Xie D (2019) Influence of impactor shape on low-velocity impact behavior of fiber metal laminates combined numerical and experimental approaches. *Thin Walled Struct* 145:106399. <https://doi.org/10.1016/j.tws.2019.106399>
 14. Guo Z, Li Z, Zhu H, Cui J, Li D, Li Y, Luan Y (2020) Numerical simulation of bolted joint composite laminates under low-velocity impact. *Mater Today Commun* 23:100891. <https://doi.org/10.1016/j.mtcomm.2020.100891>
 15. Meo M, Vignjevic R, Marengo G (2005) The response of honeycomb sandwich panels under low-velocity impact loading. *Int J Mech Sci* 47:1301–1325. <https://doi.org/10.1016/j.ijmecsci.2005.05.006>
 16. Sun G, Wang E, Wang H, Xiao Z, Li Q (2018) Low-velocity impact behavior of sandwich panels with homogeneous and stepwise graded foam cores. *Mater Des* 160:1117–1136. <https://doi.org/10.1016/j.matdes.2018.10.047>
 17. Gunes A, Sahin OS (2020) Investigation of the effect of surface crack on low-velocity impact response in hybrid laminated composite plates. *J Braz Soc Mech Sci Eng* 42:348. <https://doi.org/10.1007/s40430-020-02422-2>
 18. He W, Liu J, Wang S, Xie D (2018) Low-velocity impact behavior of X-Frame core sandwich structures—experimental and numerical investigation. *Thin Walled Struct* 131:718–735. <https://doi.org/10.1016/j.tws.2018.07.042>
 19. Dai X, Yuan T, Zu Z, Ye H, Cheng X, Yang F (2020) Experimental investigation on the response and residual compressive property of honeycomb sandwich structures under single and repeated low velocity impacts. *Mater Today Commun* 25:101309. <https://doi.org/10.1016/j.mtcomm.2020.101309>
 20. Yuan B, Ye M, Hu Y, Cheng F, Hu X (2020) Flexure and flexure-after-impact properties of carbon fibre composites interleaved with ultra-thin non-woven aramid fibre veils. *Compos A* 131:105813. <https://doi.org/10.1016/j.compositesa.2020.105813>
 21. He W, Lu S, Yi K, Wang S, Sun G, Hu Z (2019) Residual flexural properties of CFRP sandwich structures with aluminum honeycomb core after low-velocity impact. *Int J Mech Sci* 161–162:105026. <https://doi.org/10.1016/j.ijmecsci.2019.105026>
 22. Sohel KMA, Jabri KA, Abri AHS (2020) Behavior and design of reinforced concrete building columns subjected to low-velocity car impact. *Structures* 26:601–616. <https://doi.org/10.1016/j.istruc.2020.04.054>
 23. Sadeghpour E, Afshin M, Sadighi M (2015) A theoretical investigation on low-velocity impact response of a curved sandwich beam. *Int J Mech Sci* 101–102:21–28. <https://doi.org/10.1016/j.ijmecsci.2015.07.011>
 24. Fan Y, Xiang Y, Shen HS, Wang H (2018) Low-velocity impact response of FG-GRC laminated beams resting on visco-elastic foundations. *Int J Mech Sci* 141:117–126. <https://doi.org/10.1016/j.ijmecsci.2018.04.007>
 25. Xu L, Shi M, Wang Z, Zhang X, Xue G (2020) Experimental and numerical investigation on the low-velocity impact response of shape memory alloy hybrid composites. *Mater Today Commun*. <https://doi.org/10.1016/j.mtcomm.2020.101711>
 26. Nasrin S, Ibrahim A (2019) Numerical study on the low-velocity impact response of ultra-high-performance fiber reinforced concrete beams. *Structures* 20:570–580. <https://doi.org/10.1016/j.istruc.2019.06.011>
 27. Manohar T, Suribabu CR, Murali G, Salaimanimagudam MP (2020) A novel steel-PAFRC composite fender for bridge pier protection under low velocity vessel impacts. *Structures* 26:765–777. <https://doi.org/10.1016/j.istruc.2020.05.005>
 28. Hosseini H, Kolahchi R (2018) Seismic response of functionally graded-carbon nanotubes-reinforced submerged viscoelastic cylindrical shell in hygrothermal environment. *Phys E* 102:101–109. <https://doi.org/10.1016/j.physe.2018.04.037>
 29. Cong PH, Khanh ND, Khoa ND, Duc ND (2018) New approach to investigate nonlinear dynamic response of sandwich auxetic double curves shallow shells using TSDT. *Compos Struct* 185:455–465. <https://doi.org/10.1016/j.compstruct.2017.11.047>
 30. Raissi H (2020) Stress distribution of a sector of cylindrical sandwich shell with FG-CNT core and piezoelectric face sheets subjected to blast pressure. *Aust J Mech Eng*. <https://doi.org/10.1080/14484846.2020.1817272>
 31. Raissi H (2020) Time-dependent stress analysis of a sector of the spherical sandwich shell with piezoelectric face sheets and FG-CNT core subjected to blast pressure. *Thin Walled Struct* 157:106864. <https://doi.org/10.1016/j.tws.2020.106864>
 32. Romera JM, Carbajal N, Mujika F (2020) A simple analytical method for determining interlaminar shear stresses in symmetric laminates. *Structures* 25:683–695. <https://doi.org/10.1016/j.istruc.2020.03.053>
 33. Malikan M, Nguyen VB (2018) Buckling analysis of piezo-magneto-electric nanoplates in hygrothermal environment based on a novel one variable plate theory combining with higher-order nonlocal strain gradient theory. *Phys E* 102:8–28. <https://doi.org/10.1016/j.physe.2018.04.018>
 34. Van PP, Thoi TN, Van HL, Hoang CT, Xuan HN (2014) A cell-based smoothed discrete shear gap method (CS-FEM-DSG3) using layerwise deformation theory for dynamic response of composite plates resting on viscoelastic foundation. *Comput Methods Appl Mech Eng* 272:138–159. <https://doi.org/10.1016/j.cma.2014.01.009>
 35. Raissi H, Shishehsaz M, Moradi S (2019) Stress distribution in a five-layer sandwich plate with FG face sheets using layerwise

- method. *Mech Adv Mater Struct* 26:1234–1244. <https://doi.org/10.1080/15376494.2018.1432796>
36. Neves AMA, Ferreira AJM, Carrera E, Roque CMC, Cinefra M, Jorge RMN, Soares CMM (2012) A quasi-3D sinusoidal shear deformation theory for the static and free vibration analysis of functionally graded plates. *Compos B Eng* 43:711–725. <https://doi.org/10.1016/j.compositesb.2011.08.009>
37. Neves AMA, Ferreira AJM, Carrera E, Cinefra M, Roque CMC, Jorge RMN, Soares CMM (2012) A quasi-3D hyperbolic shear deformation theory for the static and free vibration analysis of functionally graded plates. *Compos Struct* 94:1814–1825. <https://doi.org/10.1016/j.compstruct.2011.12.005>
38. Keleshteri MM, Asadi H, Wang Q (2017) Large amplitude vibration of FG CNT reinforced composite annular plates with integrated piezoelectric layers on elastic foundation. *Thin Walled Struct* 120:203–214. <https://doi.org/10.1016/j.tws.2017.08.035>
39. Keleshteri MM, Asadi H, Wang Q (2017) Postbuckling analysis of smart FG CNTRC annular sector plates with surface-bonded piezoelectric layers using generalized differential quadrature method. *Comput Methods Appl Mech Eng* 325:689–710. <https://doi.org/10.1016/j.cma.2017.07.036>
40. Pattanaik A, Bhuyan SK, Samal SK, Behera A, Mishra SC (2016) Dielectric properties of epoxy resin fly ash composite. *Mater Sci Eng* 115:012003. <https://doi.org/10.1088/1757-899X/115/1/012003>
41. Karunaratna P, Chithradewa K, Kumara S, Weerasekara C, Sarasinghe R, Rathnayake T (2019) Study on dielectric properties of epoxy resin nanocomposites. *IEEE Xplore*. <https://doi.org/10.1109/ISAECT47714.2019.9069694>.
42. Yang G, Li J, Ohki Y, Wang D, Liu G, Liu Y, Tao K (2020) Dielectric properties of nanocomposites based on epoxy resin and HBP/plasma modified nanosilica. *AIP Adv* 10:045015. <https://doi.org/10.1063/1.5103237>
43. Wang JH, Liang GZ, Yan HX, He SB (2008) Mechanical and dielectric properties of epoxy/dicyclopentadiene bisphenol cyanate ester/glass fabric composites. *eXPRESS Polym Lett* 2:118–125. <https://doi.org/10.3144/expresspolymlett.2008.16>
44. Baba MN, Dogaru F, Guiman MV (2020) Low velocity impact response of laminate rectangular plates made of carbon fiber reinforced plastics. *Procedia Manuf* 46:95–102. <https://doi.org/10.1016/j.promfg.2020.03.015>

Publisher's Note Springer Nature remains neutral with regard to jurisdictional claims in published maps and institutional affiliations.